Transactions of Tianjin University (2024) 30:178–197
https://doi.org/10.1007/s12209-024-00392-3

REVIEW

Review of Iron-Based Catalysts for Carbon Dioxide Fischer–Tropsch Synthesis

Ji-Yue Jia[1] · Yu-Ling Shan[2] · Yong-Xiao Tuo[1] · Hao Yan[1] · Xiang Feng[1] · De Chen[3]

Received: 21 December 2023 / Accepted: 24 January 2024 / Published online: 9 April 2024

Abstract

Capturing and utilizing CO_2 from the production process is the key to solving the excessive CO_2 emission problem. CO_2 hydrogenation with green hydrogen to produce olefins is an effective and promising way to utilize CO_2 and produce valuable chemicals. The olefins can be produced by CO_2 hydrogenation through two routes, i.e., CO_2-FTS (carbon dioxide Fischer–Tropsch synthesis) and MeOH (methanol-mediated), among which CO_2-FTS has significant advantages over MeOH in practical applications due to its relatively high CO_2 conversion and low energy consumption potentials. However, the CO_2-FTS faces challenges of difficult CO_2 activation and low olefins selectivity. Iron-based catalysts are promising for CO_2-FTS due to their dual functionality of catalyzing RWGS and CO-FTS reactions. This review summarizes the recent progress on iron-based catalysts for CO_2 hydrogenation via the FTS route and analyzes the catalyst optimization from the perspectives of additives, active sites, and reaction mechanisms. Furthermore, we also outline principles and challenges for rational design of high-performance CO_2-FTS catalysts.

Keywords CO_2 hydrogenation · Olefins · CO_2-FTS · Iron-based catalysts

Introduction

In recent years, carbon neutrality has gained significant attention, and global efforts have been devoted to mitigating CO_2 emissions. Due to its abundance and nontoxicity, the conversion of CO_2 into value-added products is an attractive approach to addressing the issue of CO_2 storage and sequestration and reducing dependence on fossil fuels by using CO_2 as feedstock for various processes [1–3]. Because CO_2 is very stable, its conversion into high-value-added products is challenging [4, 5]. Among various methods for CO_2 hydrogenation, thermal catalysis, photocatalysis, and electrocatalysis are the most promising approaches [6–8]. Particularly, thermal catalytic CO_2 hydrogenation for olefin production has recently made significant strides [9]. As important raw materials, olefins are traditionally produced by the petrochemical industry, and it was predicted that in 2022, the total global ethylene production capacity alone would reach 218 million tons, which would lead to more than 20 billion tons of CO_2 emissions [10, 11]. Therefore, direct synthesis of light and heavy olefins from CO_2 is a promising approach to achieve CO_2 neutralization.

CO_2 hydrogenation to olefins proceeds through two routes, namely the methanol route and the CO_2-FTS route (Fig. 1). The methanol route is through the conversion of CO_2 into methanol using the carbon-to-methanol process and then methanol into olefins using the methanol-to-olefins (MTO) technology. The catalysts used for the methanol route are typically bifunctional catalysts that comprise a metal/oxide component for methanol synthesis and a zeolite component for the MTO process, which can directly convert CO_2 into olefins [5]. Meanwhile, the CO_2-FTS route combines the reverse water–gas shift (RWGS) reaction and the Fischer–Tropsch synthesis (FTS) reaction. Similarly, the catalysts for the CO_2-FTS route also have two active sites, one for the RWGS reaction and one for the FTS reaction [1, 4, 5, 12, 13]. For CO_2 to olefins through the CO_2-FTS route, the

✉ Yu-Ling Shan
shanyl@qust.edu.cn

✉ Xiang Feng
xiangfeng@upc.edu.cn

[1] State Key Laboratory of Heavy Oil Processing, China University of Petroleum, Qingdao 266580, China

[2] College of Chemical Engineering, Qingdao University of Science and Technology, Qingdao 266042, China

[3] Department of Chemical Engineering, Norwegian University of Science and Technology, 7491 Trondheim, Norway

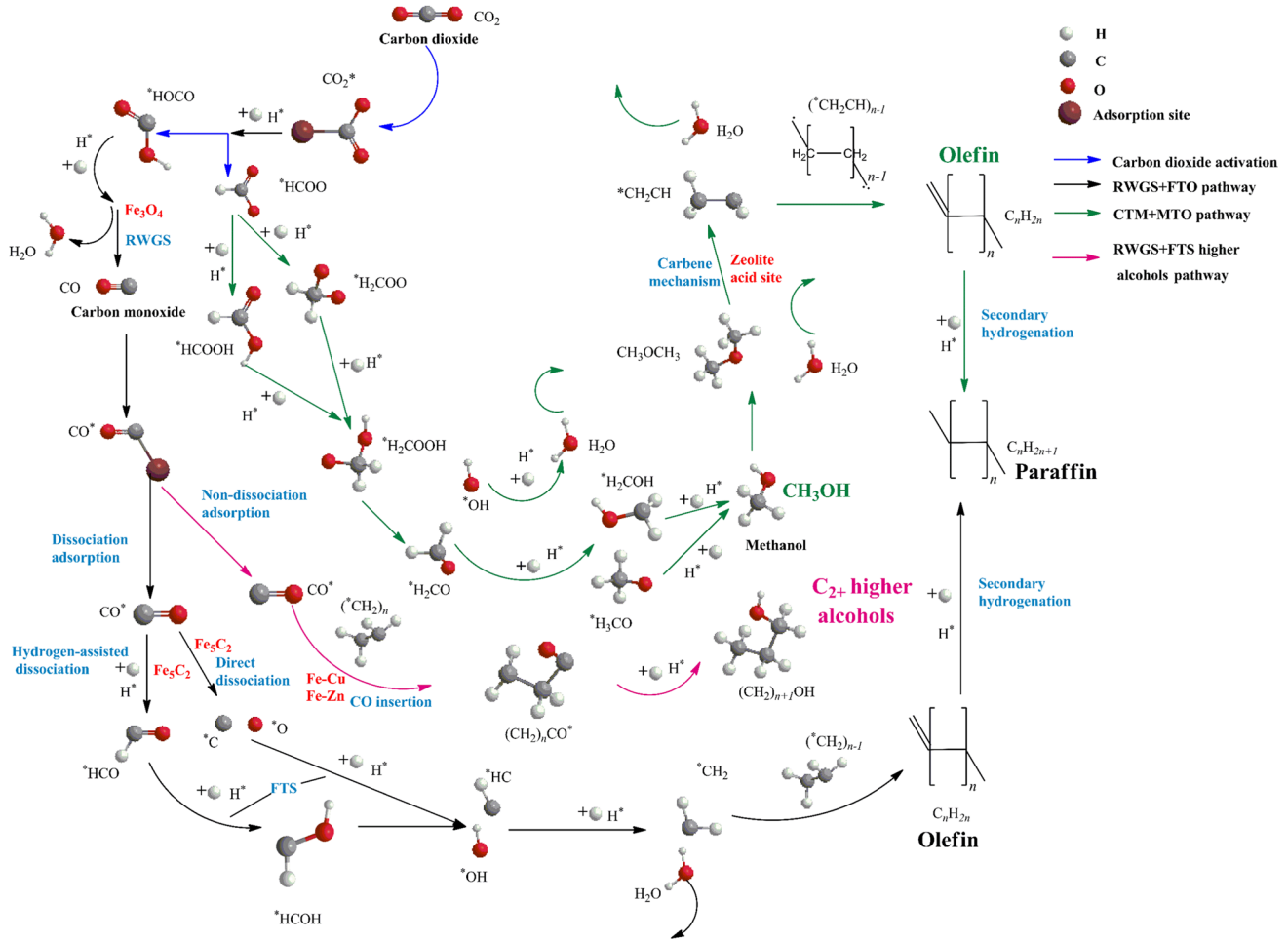

Fig. 1 Two pathways of CO_2 hydrogenation to olefin

RWGS reaction is endothermic, while the FTS reaction is exothermic, and thus, the CO_2-FTS route is thermodynamically more favorable by combining these two reactions. Furthermore, the FTS reaction consumes CO, which shifts the equilibrium of the RWGS reaction to the right and enhances CO_2 conversion [12, 13]. In addition, it has been shown that by regulating the active sites of catalysts, the CO_2-FTS route could possibly deviate from the Anderson–Schulz–Flory distribution, which opens an opportunity to achieve higher olefin selectivity. Therefore, the CO_2-FTS route is more favorable for practical applications due to its high efficiency in CO_2 conversion, selectivity, and energy utilization.

CO_2 activation remains a major challenge in CO_2-FTS compared with conventional CO-FTS [14, 15]. CO_2-FTS catalysts typically exhibit a higher surface H/C ratio than CO-FTS catalysts, which can reduce the chain propagation ability and increase methane formation. Moreover, the low partial pressure of CO can enhance the secondary reactions of olefins, leading to the formation of more saturated hydrocarbons. Therefore, efficient CO production from RWGS is crucial for the production of olefins through FTS [16–18]. To overcome these challenges, there is a need for improved adsorption and activation of CO_2, as well as enhanced C–C coupling, to obtain olefins with higher carbon numbers. In addition, there is a need to increase the selectivity toward olefins while suppressing the formation of C_1 species and alkanes and improving the stability of the catalyst to prevent catalyst sintering and carbon deposition [10, 11, 16–20]. Therefore, a rational design of catalysts is essential to achieving high-efficiency CO_2 conversion to olefins.

Transition metal-based catalysts, such as Fe, Co, and Ru, are commonly used in CO_2-FTS. Co-based catalysts are highly active and preferentially produce linear hydrocarbons but suffer from low RWGS activity. Ru-based catalysts exhibit good activity at low temperatures but have low RWGS activity and are expensive [14]. Meanwhile, Fe-based catalysts are cheap, versatile, and highly efficient in catalyzing the RWGS reaction, which draws significant attention for

their use in CO_2 conversion through the Fischer–Tropsch synthesis pathway.

Recently, various promoters such as N, Co, and Cu have been examined to improve the catalytic efficiency of Fe-based catalysts [21–23]. The active phases of Fe-based catalysts for RWGS and FTS are reported to be iron oxide (Fe_3O_4) and iron carbide (Fe_5C_2) [24]. For example, the introduction of transition metals such as Cu, Zn, and Co can enhance the carbon chain growth, likely due to the enhanced formation and distribution of Fe_5C_2 through metal–metal interaction [22], which improves the C–C coupling ability [21, 22, 25]. The introduction of alkali metals such as Na and K can increase the olefin selectivity, likely due to the increased surface alkalinity caused by the alkali metals, which enhances CO_2 adsorption and suppresses H_2 activation, leading to an increased surface C/H ratio [1–3, 26–30]. Moreover, the introduction of alkaline earth metals such as Sr can promote the dispersion of Fe active sites and facilitate the formation and stabilization of Fe_5C_2 phases. Moreover, Sr can enhance the electron interaction between Na and Fe species, leading to a synergistic effect that improves the C–O dissociation adsorption and the subsequent C–C coupling [30, 31].

CO_2 conversion has been reviewed extensively. Wang et al. [11] discussed the reaction mechanisms of CO_2 hydrogenation through CO_2-FTS and MeOH routes and the optimization of reaction conditions. Meanwhile, the main focus of Sun et al. [32] was on spinel ferrite-based catalysts for CO_2 hydrogenation to fuel-related chemicals. In contrast to previous reports, this review mainly focuses on Fe-based catalysts and their role in CO_2 conversion through the CO_2-FTS route (Fig. 2). The effects of various promoters, nature of active sites, and reaction mechanisms are included and discussed comprehensively, with the goal of providing insights into the rational design of high-efficiency CO_2-FTS catalysts [33].

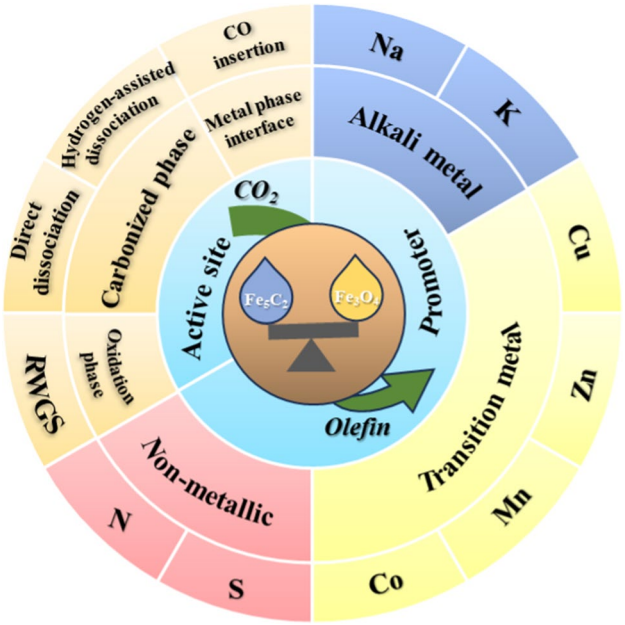

Fig. 2 Scope and contents of the review on iron-based catalysts for CO_2-FTS

Promoters for Iron-Based Catalysts

Alkali Metal Promoters

The selectivity of olefins can be significantly enhanced by introducing alkali metals into catalysts. Sodium and potassium are common choices, as they can donate electrons and create an alkaline surface environment. This would facilitate the adsorption of CO_2, raise the surface C/H ratio, and inhibit the adsorption of olefins [9, 34–36]. Moreover, the addition of electrons to Fe can strengthen the Fe–C bond, contributing to the formation of iron carbide active sites [1–3, 9, 12, 26–29, 34, 36]. In addition, both Na and K can cause the isomerization and hydrogenation of alpha-olefins, leading to more branched-chain alkanes (Fig. 3). Compared to Na, K-doped samples had a higher linear/branched hydrocarbon ratio, suggesting that K had lower isomerization activity [1].

The use of Na- and K-doped zinc-iron catalysts has been shown to improve the apparent reaction rate and yield of C_{2+} linear olefins for both CO and CO_2 under the same conditions [1]. The Na/Fe–Zn catalyst exhibited a higher apparent reaction rate and yield of C_{2+} linear olefins compared to the K/Fe–Zn catalyst. This suggests that Na can create a suitable balance between oxides and carbides, which is beneficial for producing long-chain olefins, especially C_{5+} olefins. This balance enhances the conversion of CO and CO_2 and increases the number of active sites on the surface. Moreover, Tu et al. [3] showed that Na promoters could enhance the stability of Fe_5C_2 by preventing phase oxidation during the reaction process (Fig. 4). Wei et al. [29] found that Na additives can also influence the particle size of Fe_2O_3 and Fe_3O_4, which can reduce the particle size of Fe_5C_2 during the CO reduction process.

It was reported that K also provides more electrons than Na during the reaction and promotes more carbide formation [1]. However, K also has higher hydrophilicity than Na, which causes strong physical adsorption of H_2O on K_2O. This may interfere with the adsorption of CO on iron carbides and affect the conversion rate. Guo et al. [2] showed that K tends to accumulate on the surface during the reaction. These surface-accumulated K species may be close to the active sites of iron carbide, providing active sites for activating C = O and coupling C–C bonds, and the surface-accumulated K was found more effective in

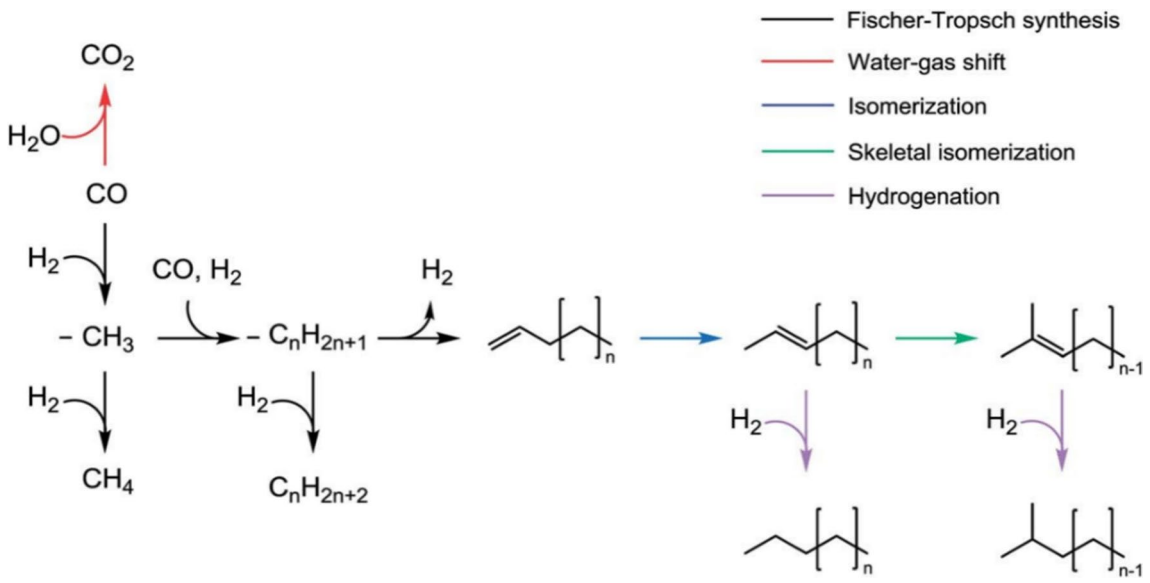

Fig. 3 Secondary reaction pathways of Na- and K-iron-based catalysts. Reproduced with permission from Ref. [44]. Copyright 2015, American Chemical Society

promoting carbide formation than dispersed K [36]. In the study conducted by Kim et al. [9], they found that in mesoporous $CuAl_2O_4$-supported Fe catalysts, a small amount of K does not significantly improve CO_2 conversion and C_{5+} selectivity. A noticeable effect can be seen only with a larger loading amount (3 wt%). This is due to changes in the amphoteric properties of the catalyst surface, which affect the binding of CO_2 and change the activation energy for electron transfer between CO_2 and the catalyst surface [37]. According to Xu et al. [28], Na affects Fe–Mn catalysts by interfering with the contact between MnO_x and Fe_2O_3 in the oxide precursors of FeMnNa catalysts, thus weakening the inhibition effect of MnO_x on the reduction of Fe_2O_3. However, excessive alkali metals such as Na and K can significantly reduce the activity of Fe-based catalysts, which in turn results in excessive reduction of Fe due to their electron-donating ability, resulting in carbon deposition and the coverage of active sites on the catalyst surface [1, 9]. Moreover, excessive alkali metals enhance the surface alkalinity of the catalyst, making it difficult for olefins to adsorb, hampering carbon chain elongation, and affecting selectivity [27, 37].

Transition Metals and Oxides

Copper and Its Oxides

Copper doping can help reduce the catalysts and form active phases like Fe_3O_4 and Fe_5C_2, which are active sites for CO_2 hydrogenation through the CO_2-FTS route [13, 21, 22]. The interaction between Cu and Fe was reported to speed up the Fe reduction and carburization to form more active sites [9, 13]. Besides, Cu was also reported to participate in the RWGS reaction, which increases the CO levels, contributing to olefin formation processes [9, 13, 22, 38–40].

Generally, Cu promotes CO_2 conversion and the formation of more long-chain olefins. In the study of Liu et al. [39], they compared catalysts prepared using co-impregnation and sequential impregnation methods for $FeCuK/Al_2O_3$. They discovered that C_{5+} selectivity increased monotonically with increasing Cu content until the mass fraction of Cu reached 3%. Using Fe and Cu separately could result in the relatively complete growth of the hematite phase. However, the interaction between Fe and Cu in the co-impregnation catalysts was successfully regulated, leading to stronger metal interactions compared to the sequentially prepared catalysts. Similarly, Kim et al. [9] prepared a mesoporous Fe catalyst supported on $CuAl_2O_4$ and compared it with physically mixed $22Fe3K/SiO_2$ and $CuAl_2O_4$. Both experimental data and characterization results demonstrated that the close chemical interaction between the Fe and Cu catalytic components is crucial for enhancing the CO_2 conversion rate, reducing C_1 product selectivity, and promoting C–C coupling reactions to improve C_{5+} selectivity.

Using a hydrothermal method, Zeng et al. [38] made $CuFeO_2$ catalysts that achieved high $C_{4+}^{=}$ selectivity (66.9%) and CO_2 conversion (27.3%) at atmospheric pressure (Fig. 5). They found that CO adsorbs without breaking on the Cu–Fe interface sites, and this CO^* adsorption is needed for CO insertion. The CO insertion at the Cu–Fe interface and the carbide mechanism on the carbide iron both

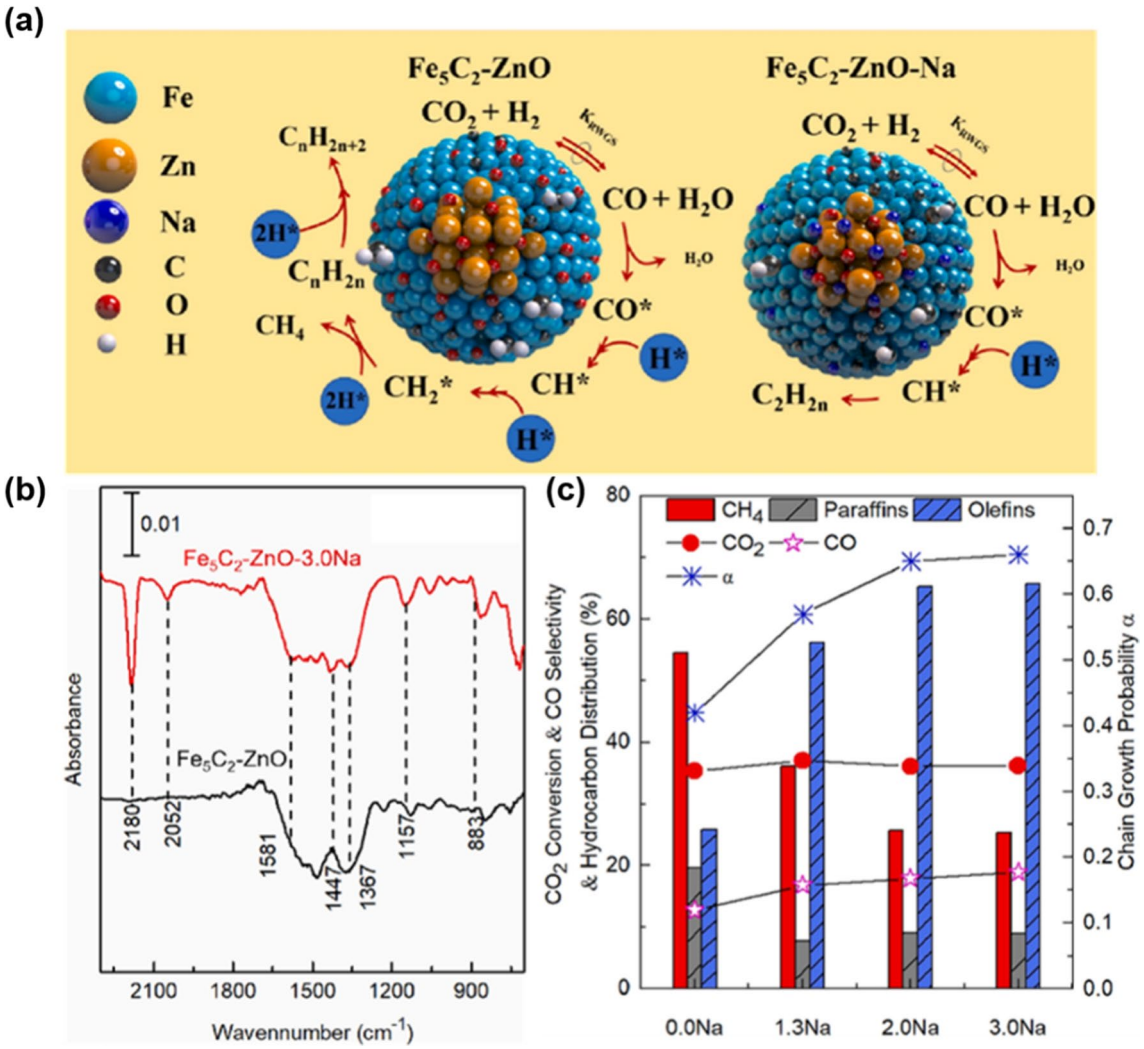

Fig. 4 **a** Possible mechanism of Na on CO_2 hydrogenation of Fe_5C_2; **b** DRIFTS spectrum of the CO reduced (10 kPa CO, 523 K, 0.83 cm^3/s) Fe_5C_2–ZnO (black line) and Fe_5C_2–ZnO–3Na (red line) catalysts after exposing to 10 kPa H_2 at 593 K for 1 h. (IR Spectrum were collected at 323 K under flowing Ar, 0.5 cm^3/s); **c** product distribution at 593 K and 1.5 MPa $H_2/CO_2 = 3$ 10 000 $cm^3/(g_{cat} \cdot h)$ Reproduced with permission from Ref. [3]. Copyright 2021, Elsevier

lead to high $C_{4+}^{=}$ selectivity. They also studied the deactivation and regeneration of the catalysts and showed that the separation and re-diffusion of Cu and Fe elements cause deactivation, which could be inhibited at high-pressure reaction conditions. Choi et al. [41] investigated the impact of synthesis methods on the performance of $CuFeO_2$ catalysts. They discovered that the duration of the hydrothermal reaction significantly influences the crystal structure of $CuFeO_2$. As the hydrothermal duration extends from 6 to 24 h, there is a gradual decrease in the intensity of impurity phases such as Fe_2O_3 and Cu_2O. The nature of the precursor plays a pivotal role during the reduction process. In the spinel $CuFe_2O_4$, both metals exist in a fully oxidized state as Cu^{2+} and Fe^{3+}. However, in $CuFeO_2$, Cu is in an intermediate oxidation state of Cu^+, which may be less thermodynamically stable to reduction. In contrast, within the FeAlK system, the composition of Fe carbides increases with an increase in Cu content. Furthermore, Cu has proven effective in producing oxygen-containing substances [21].

However, different observations for the roles of copper were also reported. Cai et al. [22] synthesized $CuFe_2O_4$-K catalysts using Prussian Blue Analogue (PBA). They found that, although with the highest selectivity toward C_{5+} products (85.50%), the incorporation of Cu was found to significantly reduce CO_2 conversion. Characterization results suggested that severe sintering of the Fe–Cu particles could be a contributing factor to the low CO_2 conversion rate. Yang et al. [13] prepared FeCu–Na catalysts in which Fe and Cu exhibited significant phase separation. The distribution of Cu was more concentrated, inhibiting C–C coupling and

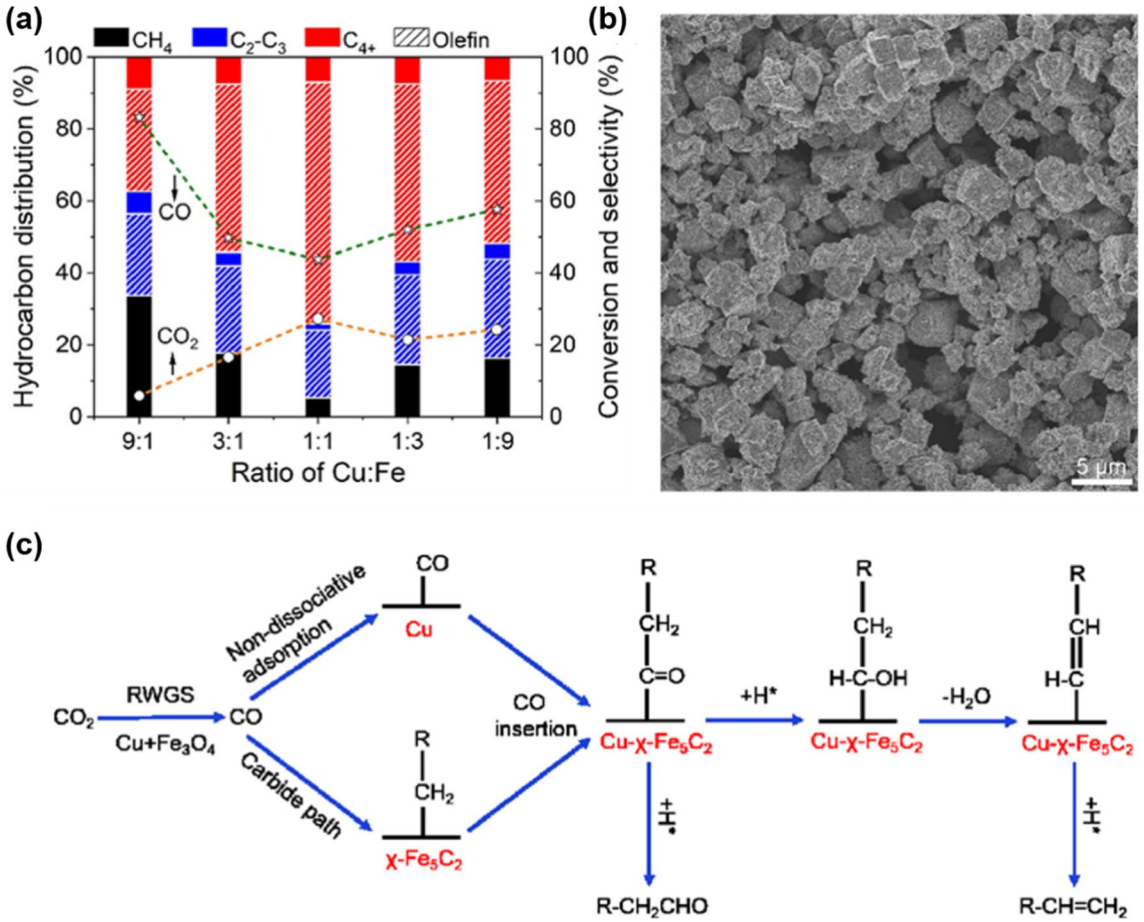

Fig. 5 **a** CO_2 conversion and product selectivity of activated Cu–Fe binary oxides with different Cu:Fe ratios. Reaction conditions: 320 °C, 0.1 MPa, $H_2/CO_2 = 3:1$, and 2 400 mL/(g_{cat}·h). Time on stream = 4 h. **b** SEM image of activated $CuFeO_2$; **c** schematic illustration of C–C coupling on the surface of activated $CuFeO_2$ Reproduced with permission from Ref. [38]. Copyright 2022, Springer Nature

decreasing the selectivity toward long-chain hydrocarbons. Moreover, Cu was reported to act as an electron promoter, enhancing the surface basicity of the catalyst. And, the inclusion of Cu significantly improved the activation of H_2 and enhanced the secondary olefin hydrogenation capability, resulting in an O/P ratio noticeably lower than other catalysts.

Zinc and Its Oxides

The introduction of Zn improves the performance of the catalyst in several ways. First, it facilitates CO_2 adsorption, activation, CO adsorption, and hydrogen dissociation [22, 23, 42, 43]. Second, it creates a strong interaction between Fe and Zn to prevent the aggregation of iron species, stabilize carbide iron, and enhance C–C coupling capability. The Zn also acts as electron-donating groups to create a surface alkaline environment and suppress secondary hydrogenation of olefins [13, 22, 23, 25, 44].

Zn could be introduced in Fe-based catalysts by a simple co-precipitation method [13]. The introduction of Zn was found to improve the dispersion of Fe species and reduce the iron particle size, which facilitates the formation of active phases such as Fe_3O_4 and Fe_5C_2 (Fig. 6) [45]. Moreover, Zn forms a $ZnFe_2O_4$ spinel structure with Fe, which strengthens the interactions between Fe and Zn and prevents the aggregation of iron carbides and iron oxides during the initial structural evolution. Zn also enhances the activation of H_2, which suppresses the oxidation of Fe_5C_2. These factors result in the remarkable stability of FeZn-based catalysts.

In the study of Zhang et al. [46], they prepared a Zn-doped Fe-based catalyst, which transformed into Fe_5C_2 and ZnO species after reduction. The ZnO species enhanced the adsorption of CO_2 and CO, facilitated the generation of new active sites on Fe_5C_2 for CO_2 activation, and enhanced the chemical adsorption and dissociation of CO. The strong adsorption of CO inhibited the adsorption of H_2, delaying the hydrogenation of surface intermediates and favoring the

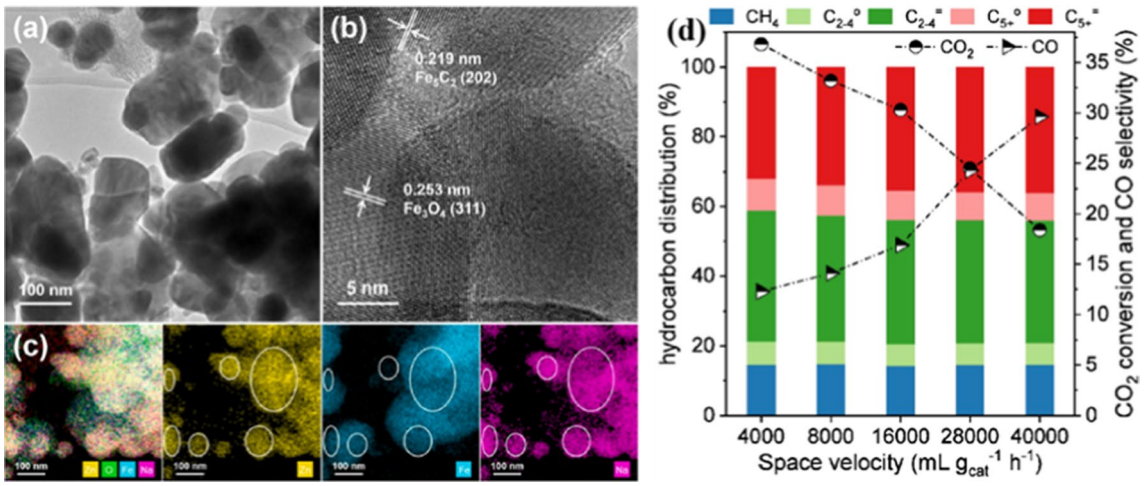

Fig. 6 **a** TEM; **b** HRTEM image; **c** EDX element map of waste FeZn–Na catalyst; **d** effect of space velocity on the catalytic performance over the FeZn–Na catalyst. Reaction conditions: 320 °C, 3 MPa, $H_2/CO_2 = 3$ Reproduced with permission from Ref. [13]. Copyright 2023, Elsevier

formation of olefins and C–C coupling intermediates (–CH_2 groups). The electron donation from Zn species also made olefins more easily desorbed on Fe–Zn catalysts, resulting in a significant decrease in their secondary hydrogenation ability. Xu et al. [25] prepared Fe/Zn/Al–Na catalysts through co-precipitation (Fig. 7). The catalyst promoted by Zn and Al exhibited better stability. Zn existed in the form of spinel in $Fe_6Zn_1Al_1$, while in Fe_3Zn_1, it existed in the form of ZnO. Fe_3Zn_1 had a higher proportion of Fe_xC due to the strong stabilizing ability of Zn toward Fe_xC. Zn and Al exhibited synergistic effects by retaining the positive effect of Al while removing the Fe–Al spinel layer. This removal of spatial hindrance on the Fe_5C_2 surface by the Fe–Zn–Al spinel, which did not encapsulate Fe_5C_2 particles, improved the selectivity to α-olefins.

When Zn is introduced into FeAlK using the impregnation method [21], the reduced catalysts consist of ferrites, regardless of the Zn content (Fig. 8). Ferrites account for over 70% of the total composition and possess alkaline sites that greatly promote carbon–carbon coupling. Zn increases the adsorption strength and enhances the carbon–carbon coupling rate, favoring the production of long-chain hydrocarbons. Thus, Zn–FeAlK tends to generate more long-chain hydrocarbons than FeAlK. The doping of Zn in the zinc-iron spinel catalyst prepared from PBAs (Prussian Blue analogs) increases the difficulty of catalyst reduction but also promotes the dispersion of catalyst particles, significantly reducing their size. The strong interaction between iron species and Zn contributes to the excellent performance of Zn–Fe catalysts (Fig. 9) [22].

The effects of calcination temperature on the performance of $Na_{0.2}/Fe_1Zn_{1.2}O_x$ catalyst were investigated by Yang et al. [44]. They found that catalysts calcinated at 400 °C exhibited smaller crystal sizes and lower total surface basicity. However, this catalyst also tended to convert α-olefin selectivity into branched alkanes. Wu et al. [43] prepared a layered K–Fe–Zn–Ti catalyst using high-temperature solid-phase reaction. They found that the interaction between Zn and Ti is weak. After Zn introduction, a stable $ZnFe_2O_4$ phase was formed, and the surface K content was significantly reduced, which facilitates the adsorption of CO_2, contributing to higher CO_2 conversion.

Manganese and Its Oxides

Manganese also has a strong interaction with iron, which inhibits the formation of iron carbide and enhances the reducibility of iron oxide. Therefore, manganese can improve the activity and selectivity of iron catalysts for various reactions. In addition, manganese also reduces the adsorption capacity of H_2 on iron surfaces. This can prevent hydrogen poisoning and increase the stability of iron catalysts [13, 28, 47–49].

For the FeMn–Na catalyst prepared by the co-precipitation method [13, 28, 47], it was found that the introduction of Mn significantly enhances the dispersion of Fe species, reduces the average grain size, and improves the reducibility of iron oxide. Mn possesses stronger reducibility compared to iron oxide and can assist in the removal of adsorbed oxygen species on the Fe surface through the overflow of oxygen vacancies in manganese oxide. The reduced catalyst contains $FeMnO_x$, indicating a close interaction between Fe and Mn. However, the strong interaction between Mn and Fe inhibits the interaction between Fe and CO, hindering the carburization of Fe and impeding the further conversion of CO intermediates. Therefore, the presence of single Mn suppresses the activity of Fe catalysts. To overcome this problem, some studies have introduced other promoters to

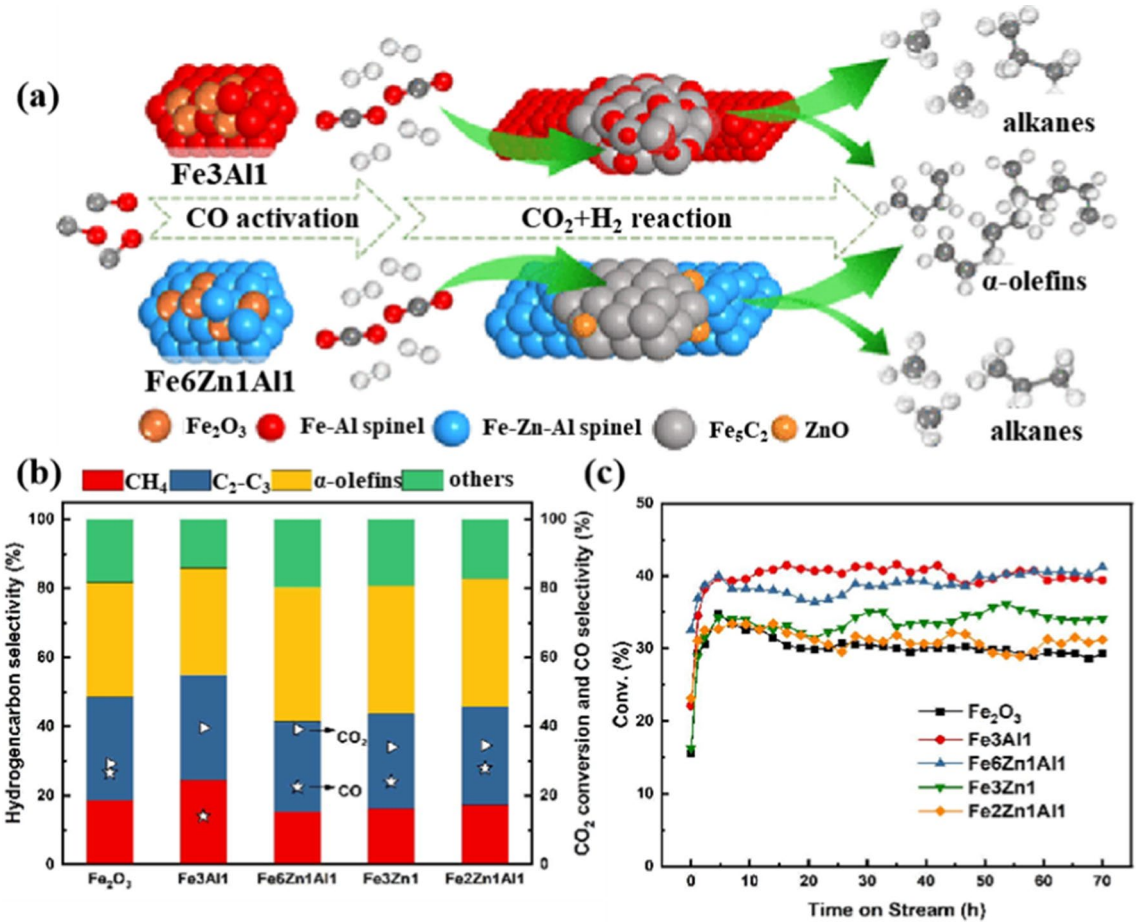

Fig. 7 **a** Reaction mechanism; **b, c** Catalyst performance. Reaction condition (330 °C, 1.5 MPa, $H_2/CO_2 = 3:1$, and 15,000 mL/(g_{cat}·h)) Reproduced with permission from Ref. [25]. Copyright 2021, ACS Publications

modify the interaction between Fe and Mn and enhance the catalytic performance. For example, Praewpilin et al. [48] prepared a K/Mn/Fe/NCNT catalyst loaded on nitrogen-doped carbon nanotubes. The manganese and potassium promoters were coated on carbon nanotubes (MnK-CNTs) to avoid the formation of amorphous MnO_x phases that could block the iron phase. In contrast, Liang et al. [49] prepared Mn-modified Na/Fe catalysts, where the addition of Mn to the Na/Fe catalysts contributes to the formation of active Fe_5C_2 species. There is a strong interaction between Mn promoter and Fe species, which lowers the quantity and strength of CO adsorption, thereby helping to weaken the chain growth reaction and leading to high selectivity for light olefins.

Cobalt and Its Oxides

Cobalt (Co) is a traditional active metal in Fischer–Tropsch synthesis (FTS), a process that converts carbon monoxide (CO) and hydrogen (H_2) into liquid hydrocarbons. Co was also found to be available in CO_2-FTS[50]. In recent years, Fe–Co catalysts with excellent performance have been reported for CO_2-FTS. The introduction of Co can significantly decrease the particle size of the catalyst [2, 21, 42, 51], improving the reduction and adsorption of CO_2 molecules [52]. Furthermore, Co facilitates the formation of electron-rich Fe_5C_2, which enhances the electron density of carbides and strengthens the Fe–C bond while weakening the C–O bond. This can effectively enhance the catalytic performance of Fe–Co catalysts for CO_2-FTS [42, 52]. Guo et al. [2] prepared a supported bimetallic catalyst using iron and cobalt on Y zeolite modified by potassium ion exchange and found that the introduction of Co prompts the formation of more carbides, contributing to the improvement in selectivity toward heavy olefins. In the FeAlK system [21], introducing Co through co-precipitation would lead to the formation of heterogeneous Co metal in the iron lattice, resulting in defects and a reduction of iron crystal size.

Moreover, the presence of Co also enhances the adsorption of H_2 due to its strong H bonding energy [53]. However, it also hinders the migration of surface H to neighboring Fe species. In contrast, the $CoFe_2O_4$-K

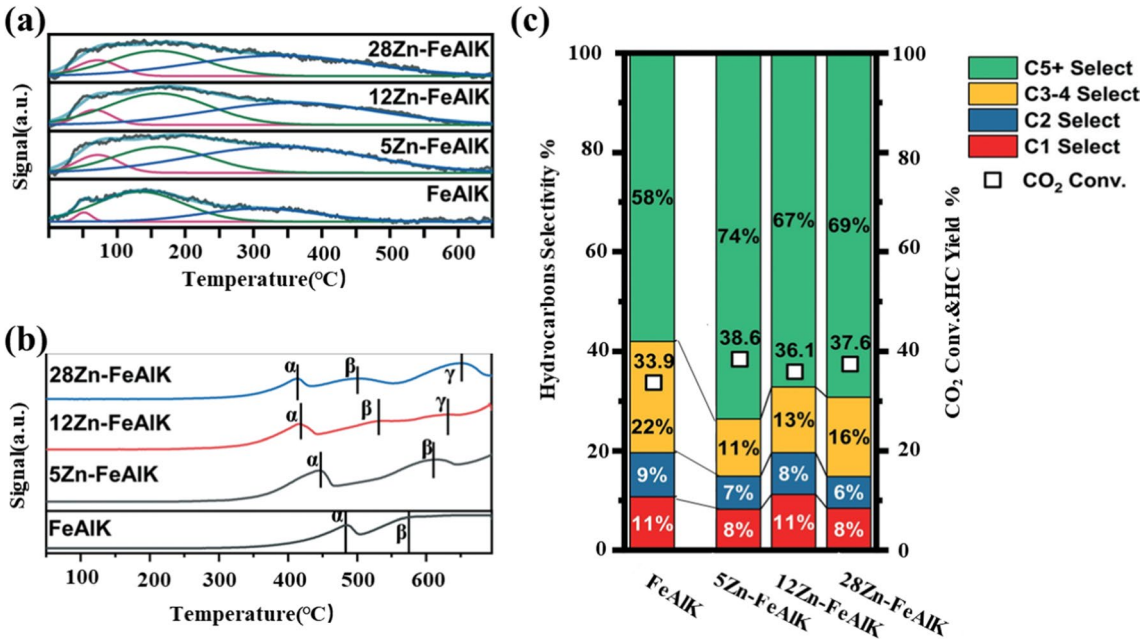

Fig. 8 **a** CO_2-TPD profiles of the catalyst samples; **b** H_2-TPR profiles of the catalyst samples; **c** Zn–FeAlK catalyst performance Reproduced with permission from Ref. [21]. Copyright 2022, Royal Soc Chemistry

catalyst prepared using a Prussian blue analog (PBA) as a precursor exhibits good selectivity toward C_{2-4} olefins (Fig. 9) [22]. Guo et al. [42] employed co-precipitation to introduce both zinc (Zn) and Co into Fe-based catalysts. A spinel structure of K-Zn$(FeCo)_2O_4$ was synthesized, which exhibited remarkably high activity (60.4%) and low CO selectivity (4.5%). The doping of Co metal enhanced the utilization of carbon elements and resulted in higher olefin yields. The KZFe-Co catalyst was further synthesized using a carbon template method [52]; with the introduction of Co, the cascade reaction between the reverse water–gas shift (RWGS) and chain propagation was significantly enhanced, and the CO_2 adsorption strength increased notably. Co and Fe were found to form an alloy phase (Co_3Fe_7) during the reaction, which improves the CO_2 adsorption and promotes the formation of oxygen-containing species (CO^*, $HCOO^*$, CO_3^{2*}, and HCO_3^*), which can further support chain propagation through the oxygenation reaction mechanism.

However, there is competition between methane formation and the generation of oxygen-containing functional groups, and an excess amount of Co can hinder the production of long-chain products [52]. When Co is used alone in CO_2-FTS, it exhibits a high tendency for methane formation. Therefore, when Fe and Co are used together, they may enhance the selectivity toward paraffins and suppress the production of olefins, attributing to the properties of Co promoting the hydrogenation of surface CH species, which lowers the probability of chain growth [54]. The conversion of CO_2 was found to increase with increasing Co content in iron-based catalysts. However, the intrinsic methane formation activity of Co can lead to a decrease in selectivity toward long-chain hydrocarbons (C_{5+}) while increasing the selectivity toward light hydrocarbons (C_{1-4}). Therefore, the optimal amount of Co addition is crucial for achieving high performance. When a small amount of Co is added (5Co-FeAlK), Co atoms can be well integrated into the Fe structure, and the methane formation activity is not significant [55, 56]. On the other hand, when a larger amount of Co is added (12Co- and 28Co-FeAlK), the Co atoms in the FeCo alloy are likely to form clusters, accelerating the hydrogenation of surface CH_x species and leading to methane production. Co-based catalysts perform poorly for CO_2 hydrogenation: they display extremely high methane selectivity [22, 53, 56, 57]. They limit the growth of carbon chains due to the presence of a single cobalt carbide phase and decrease the conversion of CO_2–CO. The interaction between Fe and Co facilitates the transformation of Fe(III) to Fe(II) and further to carbide species to improve the adsorption and activation of CO_2 and CO intermediates [2, 21, 55, 56, 58]. Co can form a Co_3Fe_7 alloy phase with Fe, which also serves as an active site for FTS.

Nitrogen and Sulfur Doping

Carbon-based support materials, such as carbon nanotubes (CNTs) and activated carbon (AC), can be modified by nitrogen doping, a common method that also enables nitrogen-doped carbon materials, such as g-C_3N_4, to serve

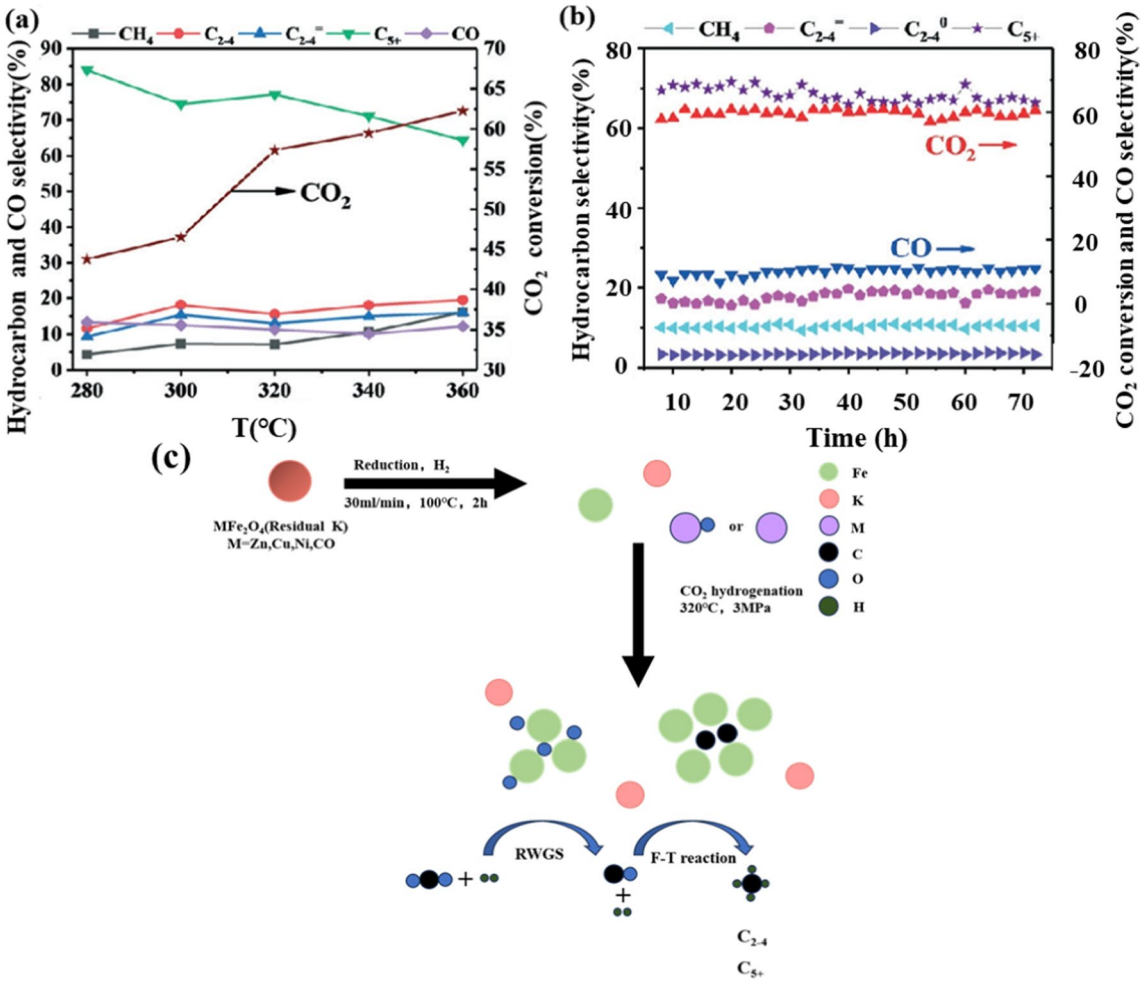

Fig. 9 **a** CO_2 hydrogenation over Zn–Fe at different temperatures. Reaction conditions: 3 MPa, $H_2/CO_2 = 3:1$, 8 h, and 12 000 mL/(g_{cat}·h); **b** stability of the bimetallic Zn–Fe catalysts. Reaction conditions: 320 °C, 3 MPa, $H_2/CO_2 = 3:1$, and 12 000 mL/(g_{cat}·h). **c** Structural evolution and mechanism of C_{5+} hydrocarbon synthesis by CO_2 hydrogenation of MFe_2O_4 (M = zinc, copper, nickel, cobalt) Reproduced with permission from Ref. [22]. Copyright 2022, Royal Soc Chemistry

as catalyst supports. Generally, nitrogen doping could enhance the surface basicity of carbon materials, which would probably contribute to improving CO_2 adsorption and suppressing the absorption and dissociation of H_2, thereby inhibiting the secondary hydrogenation of light olefins [59, 60].

Nitrogen atom doping has been reported to facilitate the reduction of iron oxides and promote the formation of active carbon phases while inhibiting crystal aggregation [23, 48, 59, 61, 62]. Chew et al. [49] used a dry impregnation method to prepare iron catalysts supported on N-functionalized multi-walled carbon nanotubes (CNTs). Their experimental results showed that iron oxide nanoparticles supported on nitrogen-doped carbon nanotubes were more easily reduced than those supported on oxygenated carbon nanotubes. Using N-functionalized carbon nanotubes (NCNTs) as support, Kangvansura et al. [48] prepared an iron-based catalyst that exhibited high reducibility due to the high dispersion of iron within the NCNTs. The NCNTs were modified with 10 mol/L nitric acid, and the nitrogen in them induced certain distortions in the carbon-iron (π-d) interaction on the curved surface of the carbon nanotubes [63]. Zhang et al. [59] synthesized Fe_3O_4–FeC_x heterogeneous catalysts with active sites confined within N-doped graphene shells on the surface of N-doped ordered mesoporous carbon (N-OMC). The nitrogen doping promoted the formation of FeC_x and inhibited crystal aggregation (Fig. 10). By modifying the surface electron density with alkali metals and nitrogen atoms, they increased the surface alkalinity, suppressed the absorption and dissociation of H_2, enhanced CO_2 adsorption, and inhibited the excessive hydrogenation of CH_x, thereby improving the yield of light olefins.

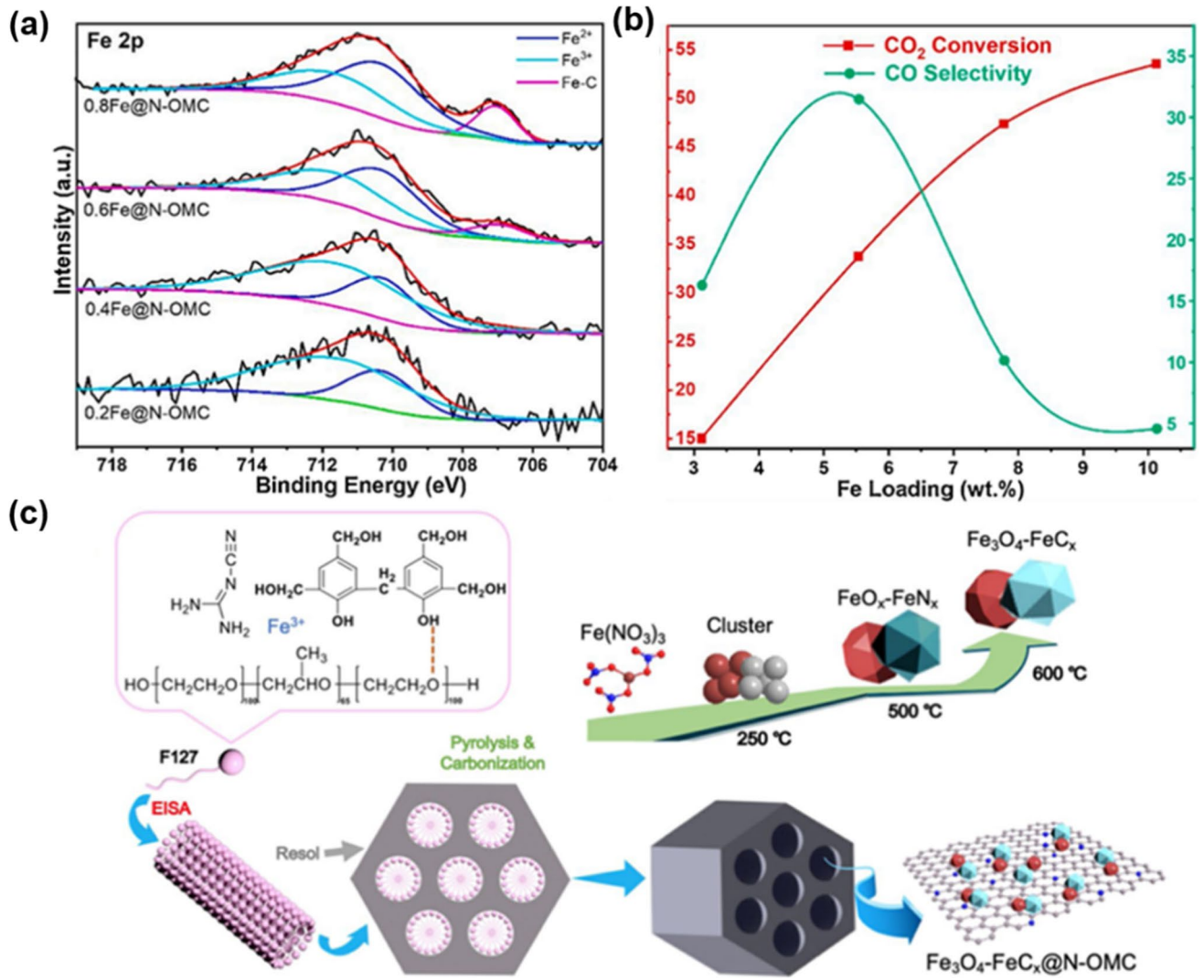

Fig. 10 Surface analysis of catalysts with different Fe loading. **a** XPS spectra of 0.2Fe@N-OMC, 0.4Fe@N-OMC, 0.6Fe@N-OMC, and 0.8Fe@N-OMC; **b** CO_2 conversion and CO selectivity of catalysts with various Fe loading; **c** schematic of the preparation process of Fe_3O_4–FeC_x@N-OMC Reproduced with permission from Ref. [59]. Copyright 2021, Elsevier

Furthermore, nitrogen doping creates a rich electron environment that weakens the adsorption strength of hydrocarbon intermediates and promotes the formation of long-chain products such as C_{5+} [55, 61]. Nitrogen atoms in pyridine-like structures have higher electron density than those in pyrrole-like structures, making them more favorable for stabilizing Fe–C bonds [62]. The improved CO_2 hydrogenation performance depends on several factors influenced by the type of nitrogen doping, such as the catalyst's specific surface area, the carbonization degree of the iron precursor, the number of defect sites, and the content of pyridine-like nitrogen structures [64]. Liu et al. [23] prepared a zinc oxide and nitrogen-doped carbon (NC)-coated iron-based catalyst, Fe@NC (Fig. 11), which showed a 25% increase in the reaction rate and a 24-fold enhancement in the O/P ratio compared to the benchmark Fe_3O_4 catalyst. This enhancement was attributed to ZnO, which is beneficial for CO_2 adsorption and hydrogen dissociation. The introduction of NC and alkaline accelerators improved the selectivity and O/P of light olefins.

Contrary to the conventional view of sulfur as a toxic component, sulfur was reported to act as a promoter for iron-based catalysts in FTS when doped at low concentrations [65]. In combination with alkali metal Na, sulfur was reported to lower methane selectivity, increase chain growth probability, enhance olefin selectivity, and facilitate the reduction and carburization of iron phases [66]. Using sulfur and sodium as promoters, Galvis et al. [65, 67] prepared iron nanoparticles uniformly dispersed on alumina or carbon nanofiber supports. The presence of sulfur was found to

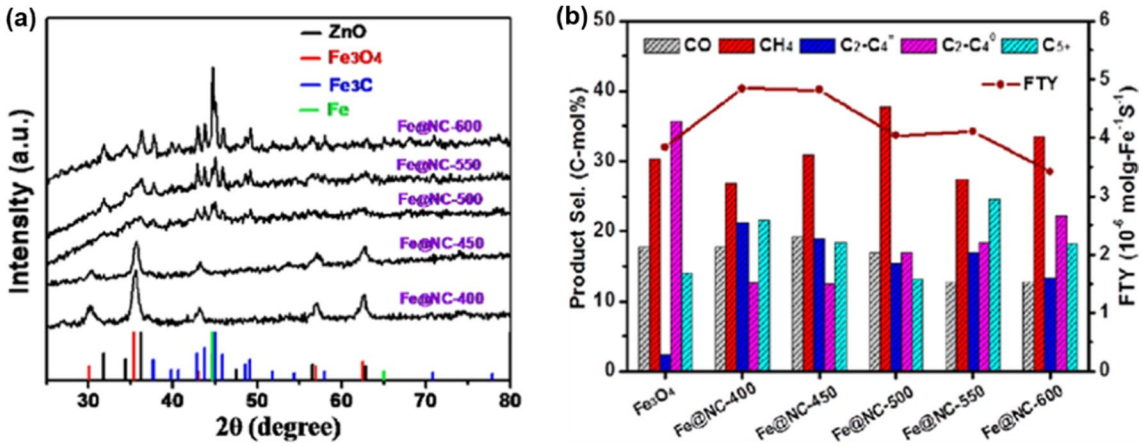

Fig. 11 **a** XRD patterns of Fe@NC; **b** FTY and product distribution over Fe_3O_4 and Fe@NC catalysts Reproduced with permission from Ref. [23]. Copyright 2019, ACS Publications

reduce methane selectivity and increase olefin selectivity by blocking the active sites for hydrogenation reactions. However, the sulfur-promoted catalysts also showed a higher degree of coking than the non-promoted samples.

Reaction Mechanism and Kinetics

Nature of Active Sites

The CO_2-FTS reaction involves two steps: the RWGS reaction, which converts CO_2 to CO on the iron oxide phase (mainly Fe_3O_4), and the subsequent CO hydrogenation FTS process, which produces hydrocarbons on the iron carbide phase (mainly χ-Fe_5C_2) [68, 69]. The composition, structure, and bonding of the iron oxide and iron carbide phases significantly affect CO_2-FTS. Before the reaction, the precursor is pretreated with H_2 or CO. The CO_2 in the reaction atmosphere and the water produced during the reaction are strong oxidizing agents, while H_2 is a reducing agent. Therefore, the catalyst undergoes drastic structural changes during reduction and reaction, making it complex to fabricate mixed iron oxide and iron carbide phases as working catalysts [70].

The dynamic equilibrium between the carbide and oxide phases is hard to control, because the final composition and structure of different phases involving iron and promoter elements depend on both the initial composition of the precursor and the activation/reaction processes [25, 29]. For most catalysts that require hydrogen activation, the oxidized phase is reduced to Fe after activation, and Fe interacts with CO_2 to form Fe_3O_4 in the early stages of the reaction. Over time, the promoter elements facilitate the in situ formation of Fe_5C_2 [21, 22, 25]. The in situ formation of Fe_5C_2 ensures the uniform distribution of the carbide phase, enabling better cooperation between the Fe_5C_2 and Fe_3O_4 active sites. Wei et al. [24] synthesized Na-Fe_3O_4 and bound it to the HZSM-5 molecular sieve to provide three types of active sites (Fe_3O_4, Fe_5C_2 and acidic sites) for the reaction, showing excellent performance (Fig. 12). Xu et al. [68] observed a significant amount of FeO_x overlayer on the χ-Fe_5C_2 main phase during the CO_2 hydrogenation process. The total RWGS rate was positively correlated with the surface content of FeO_x when the CO_2 conversion was less than 10% but negatively correlated when the CO_2 conversion was above 10%. In the latter case, the CO_2 conversion was limited by the subsequent removal of CO in FTS, which depended on the supply of surface FeC_x species. The inherent activity of RWGS is much higher than FTS. Therefore, stabilizing FeC_x through effective surface modification, either kinetically or thermodynamically, and preventing the oxidation of the carbide phase are crucial for realizing the full potential of iron-based catalysts in carbon-hydrogen compound production.

The in situ formation of carbide iron is significantly affected by the type of promoter elements and the bonding modes with iron elements. Both spinel structures [13, 21, 22, 25, 42] and perovskite structures [31] have shown good performance. Hou et al. [31] synthesized an ABO_3-type perovskite catalyst, $Sr_{1-x}K_xFeO_3$, with good thermal stability and redox activity. The introduction of K accelerated the oxygen release of $SrFeO_3$ and promoted the synchronous formation of Fe_3O_4 and Fe_5C_2. The reversibility of the perovskite catalyst ensured the high dispersion of active phases Fe_3O_4 and Fe_5C_2 within the $SrCO_3$ phase. Zhang et al. [59] synthesized a Fe_3O_4–FeC_x heterostructure and demonstrated that CO spillover on the FeO_x-FeC_x heterojunction was favored over diffusion between independent FeO_x and FeC_x species. This reduced the selectivity toward CO and improved the conversion of CO_2 and the yield of C_{2+} products. These phase interfaces

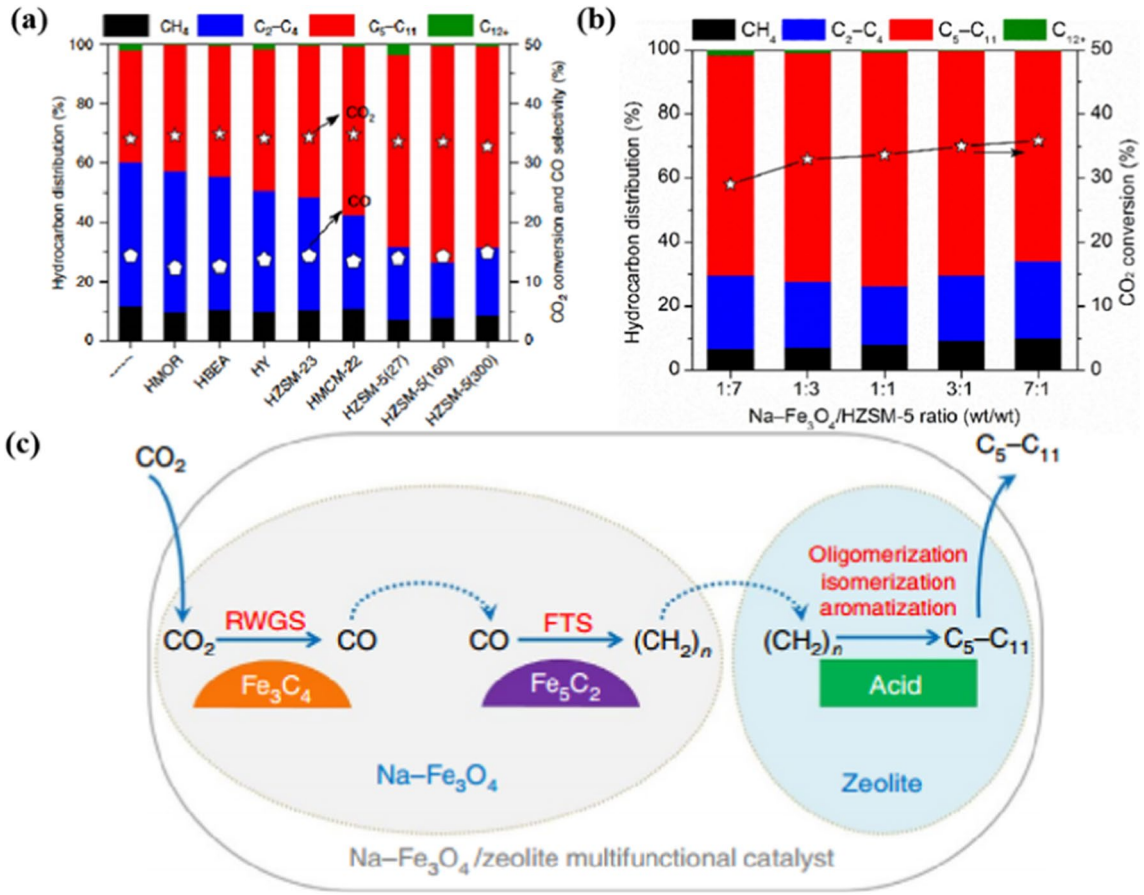

Fig. 12 **a** CO_2 conversion and product selectivity over different Na–Fe_3O_4/Zeolite catalysts; **b** catalytic performances over composite catalysts as a function of the mass ratio of Na–Fe_3O_4/HZSM-5 in the composite catalysts. reaction conditions: $H_2/CO_2 = 3$ 320 °C, 3 MPa and 4000 mL/($h \cdot g_{cat}$); **c** reaction scheme for CO_2 hydrogenation to gasoline-range hydrocarbons Reproduced with permission from Ref. [24]. Copyright 2017, Springer Nature

also exist in Cu- or Zn-promoted Fe-based catalysts, which exhibit excellent carbon chain elongation ability under higher pressure through the CO insertion mechanism, leading to the formation of oxygen-containing products in CO_2-FTS. However, Zeng et al. [38] observed that as the reaction proceeded, the distance between Fe and M metals increased, and the metal phase interface was disrupted, resulting in a significant decrease in reaction activity.

In addition, the χ-Fe_5C_2 surfaces were also reported to be capable of activating CO_2. As revealed by Nie et al. [71] by DFT calculation, they found that the χ-Fe_5C_2(510) surface exhibits higher activity for the direct dissociation of CO_2 into CO^* and O^* with a barrier of 0.24 eV, while the χ-Fe_5C_2(111) surface is more favorable for the hydrogenation of CO_2 into HCO^* intermediate with a barrier of 0.25 eV. Despite the different reaction pathways, both the (510) and (111) surfaces are good candidate surfaces for the initial activation and transformation of CO_2 (Fig. 13).

Kinetic Features of CO_2-FTS

As stated above, the hydrogenation of CO_2 over iron-based catalysts proceeds through the CO_2-FTS route, which combines the RWGS reaction and CO-FTS. The CO_2-FTS shows higher selectivity toward methane than the CO-FTS process, and the product distribution was also found to deviate from the Anderson–Schulz–Flory (ASF) distribution. As proposed by Visconti et al. [57, 72], two main reasons would account for the changes in product distributions. Firstly, the different adsorption strengths of CO and CO_2 on the catalyst surface led to different H/C ratios, which affected the chain growth ability. The relatively weak adsorption of CO_2 results in a higher H/C ratio on the catalyst surface, which promotes the hydrogenation of surface intermediates to CH_4 and reduces chain growth reactions. Secondly, as CO originates from the RWGS reaction, the surface coverage of which is relatively lower than that for the CO-FTS process, which influences the secondary reactions

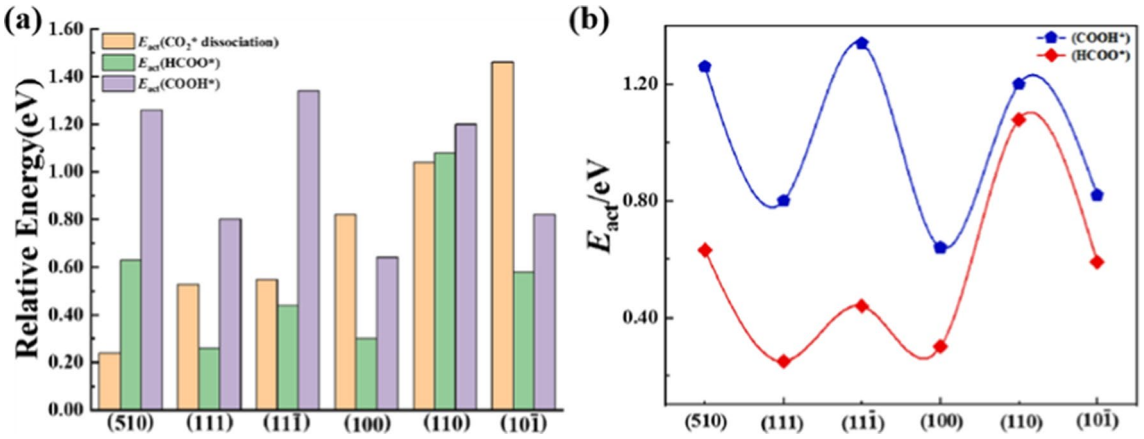

Fig. 13 **a** Comparison of Gibbs free energy barriers (673 K) for CO_2* direct dissociation; **b** CO_2* hydrogenation to HCOO* and COOH* intermediates on different surfaces of χ-Fe_5C_2 Reproduced with permission from Ref. [71]. Copyright 2022, Elsevier

of olefins, leading to more saturated hydrocarbons. Moreover, due to the involvement of two-step reactions and two types of active sites, the bonding modes of these two sites significantly influence the diffusion and adsorption of intermediates, thus affecting the overall reaction [59, 68]. Therefore, to produce olefins with high selectivity in CO_2-FTS, it is necessary to enhance the activation of CO_2 and the synergistic combination of the two reactions, in addition to traditional measures to enhance CO-FTS.

Using DFT calculations, Wang et al. [73] studied the energetically favorable pathways and the selectivity factors of hydrocarbon production from CO_2 hydrogenation. They found that the favorable pathway for CO_2 hydrogenation involves $HCOO^*$ intermediate and crucial CH^* species, which lead to the formation of CH_4 and C_2H_4, respectively. The CH^* species, passing through the HCO intermediate, is the key C_1 intermediate over χ-Fe_5C_2(510). The Microkinetic simulation results showed that CO_2 hydrogenation has higher selectivity toward CH_4 than C_2H_4, while CO hydrogenation shows the opposite trend. The main difference between CO_2 and CO hydrogenation is the different surface coverages of key species such as H^*, CH_x^*, and O^*. The higher surface coverage of O^* from CO_2 conversion occupies crucial active sites and impedes the coupling of C–C and C_2 species on χ-Fe_5C_2(510). Therefore, except for enhancing the adsorption and activation of CO_2, introducing additives such as alkaline metals and secondary transitional metals is crucial to trigger the formation and distribution of the active phases and optimization of the electronic environment of active sites to enhance the adsorption and transformation of critical intermediates [23, 59, 73].

Carbon Chain Extension Mechanism

There are two pathways for CO_2 dissociation: one is through hydrogenation of CO_2 to formate (HCOO*) intermediate, which further hydrogenates to generate methanol, and the other is through the formyl (*HOCO) intermediate, which further dissociates into $OH^*$and CO^*. The latter dominates in Fe-based catalysts [3, 11, 16]. After the formation of CO through RWGS, the CO serves as the initial surface species for further carbon chain extension reactions. Mainly two mechanism-the carbide mechanism (direct and hydrogen-assisted CO dissociation mechanism) and the CO insertion mechanism-have been reported for the activation of CO to long-chain hydrocarbons [52, 58, 74, 75].

In the CO direct dissociation mechanism, the C–O bond is directly activated to form carbides as intermediates on the surface of catalysts forms during the FTS process [76]. These carbide species undergo hydrogenation to form CH_x groups, which serve as the building blocks for alkyl chain growth [77, 78]. In this mechanism, the C between Fe and M metals increased O cleavage precedes the C–C coupling, and the coverage of CH_x groups must be high enough to favor chain growth over chain termination through hydrogenation [78]. This requires a high rate of CO dissociation. Experimental and theoretical calculations have shown that direct CO dissociation has a high energy barrier and is more difficult [79, 80]. Therefore, the hydrogen-assisted CO activation mechanism has been proposed as an alternative.

In the hydrogen-assisted CO activation mechanism, CO^* is hydrogenated to form formyl (HCO) and hydroxymethyl (HCOH) intermediates before C–O cleavage [75]. During this process, CO first reacts with H to form the formyl intermediate (*HCO). Then, the O atom of the HCO intermediate is further hydrogenated to form the

hydroxymethyl (HCOH) intermediate. Finally, the HCOH dissociates to generate the CH species, which serves as the monomer and initiator for chain growth [76, 81, 82]. It has been reported that the activation of CO through direct CO dissociation has higher activation barriers on the surfaces of Fe, Co, and Ru catalysts than that through hydrogen-assisted ones [76]. The activation mechanism of CO to form long-chain hydrocarbons depends on the exposed surface during the reaction; CO tends to be directly activated on terraced-like χ-Fe_5C_2(510) surface using the hydrogen-assisted dissociation mechanism [79], but vice versa tendency was observed over χ-Fe_5C_2(010) [80], χ-Fe_5C_2(001) [83] and χ-Fe_5C_2(100) surfaces [84].

The hydrogenation of CO^* is highly endothermic (120 kJ/mol), and the C–O activation energy (178 kJ/mol) in the hydrogen-assisted pathway is still too high to match the observed reaction kinetics [75]. Therefore, the CO insertion mechanism has been proposed [85]. In this mechanism, the RCH_x^* group couples with CO^* before C–O cleavage and directly inserts into intermediates, elongating the carbon chain. As shown in Fig. 14, this process occurs at the metal interface such as Cu–Fe [38, 41] and Co–Fe [52, 58]. Because the CO insertion process relies on non-dissociative adsorption of CO, more oxygen-containing compounds would be formed in products [38]. In general, the carbide mechanism occurs simultaneously with the CO insertion mechanism [38, 52, 86]. Which pathway is more dominant appears to depend on the nature of active sites [38, 41, 52, 58]. It was found that direct CO dissociation is more favorable than the CO insertion pathway over these ferric carbide surfaces [87]. Moreover, on the Cu–Fe or

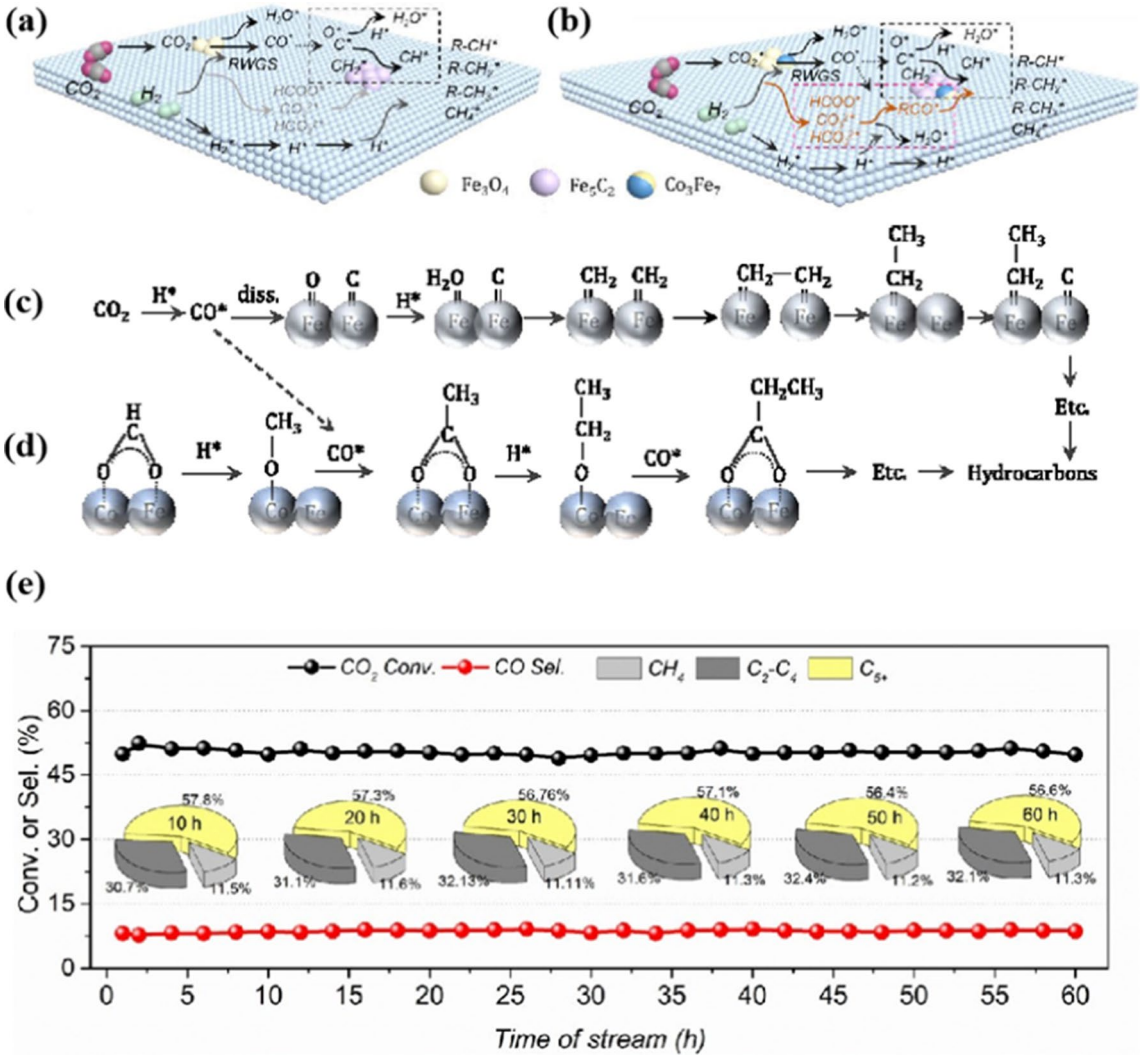

Fig. 14 **a, c** Reaction pathway for the formation of long-chain hydrocarbons through the carbide mechanism; **b, d** pathway of the oxygenated compound mechanism for the formation of long-chain hydrocarbons; **e** CO_2 hydrogenation stability over the KZFe–5.0Co catalyst at 320 °C, 2.0 MPa, 6000 mL/(g_{cat}·h) Reproduced with permission from Ref. [52]. Copyright 2022, ACS Publications

Table 1 Performances of iron-based catalysts for CO_2 hydrogenation through the CO_2-FTS route

Catalysts	H/C	Temperature (K)	Pressure (MPa)	Space velocity (mL/(g_{cat}. h))	CO_2 conversion/%	Selectivity (%)[n]				Stability/h^c	Refs
						$C_2^= - C_4^=$	CH_4	C_{5+}	CO		
Na/Fe–Zn	2	613	2	7200	26.4	23.5	10.5	54.9	11.8	200	[1]
K/Fe–Zn	2	613	2	7200	16.4	23.9	11.0	52.3	NA	200	[1]
Fe/Co–Y_K[s]	3	655	1	NA	25.9	30.2[a]	13.9	55.9[b]	21.1	100	[2]
Fe_5C_2–ZnO–3.0Na	3	593	1.5	10,000	36.2	40.4	26.2	28.8	18.9	20	[3]
22Fe3K/$CuAl_2O_4$	3	593	3	10,000	41.9	33[e]	12.5	54.5	10.2	240	[9]
layered K–Fe–Ti	3	593	2	1000[j]	35	62	24	11	NA	220	[12]
FeZn–Na	3	593	3	4000	37.5	36.9	15.0	41.3	11.5	40	[13]
FeCu–Na	3	593	3	4000	29.9	38.1	18.3	32	22.4	40	[13]
FeMn–Na	3	593	3	4000	30.2	41.9	19.2	28.5	26.3	40	[13]
10Fe0.8K0.53Co	3	573	2.5	560	54.6	24.4	18.9	47	2.0	10	[18]
10Fe0.8K1.11Co	3	573	2.5	560	57.2	23.5	22.4	43.8	1.6	10	[18]
10Fe0.8K0.53Ru	3	573	2.5	560	47.1	19.7	16.4	53.4	3.1	10	[18]
15Fe5K8Co/SiC[o]	3	573	2.5	560	30.3	14	30.8	37.1	12.3	10	[18]
15Fe5K/SiC + 8Co/SiC[p]	3	573	2.5	560	51.1	5.7	50.6	30.5	1.8	10	[18]
15Fe5K/SiC + 8Co/SiC[q]	3	573	2.5	560	49.1	0.2	79	10.3	1.8	10	[18]
15Fe5K/SiC + 8Co/SiC[r]	3	573	2.5	560	47.3	0	90.2	5.6	1.6	10	[18]
15Co/SiC	3	573	2.5	560	48.1	0	95.1	1.3	2.5	10	[18]
10Fe0.8K0.53Co	3	573	2.5	560	54.6	24.4	18.9	47	2.0	10	[18]
28Co–FeAlK	3	573	2.5	4500	45.9	37.4[e]	21.3[m]	41.2	2.6	100	[18]
28Cu–FeAlK	3	573	2.5	4500	41.2	26.9[e]	10.5[m]	62.4	2.9	100	[21]
5Zn–FeAlK	3	573	2.5	4500	38.6	17.4[e]	8.2[m]	73.8	3.1	100	[21]
FeAlK	3	573	2.5	4500	33.9	31.2[e]	10.7[m]	57.9	3.2	100	[21]
$ZnFe_2O_4$–K	3	593	3	12,000	57.4	13.1	7.2	77.2	11.8	72	[22]
$CuFe_2O_4$–K	3	593	3	12,000	32.7	7.8	4.6	85.5	16.5	NA	[22]
$NiFe_2O_4$–K	3	593	3	12,000	48.3	9.5	36.7	47.8	23.7	NA	[22]
$CoFe_2O_4$–K	3	593	3	12,000	53.0	22.6	14.6	58.1	11.3	NA	[22]
K/Fe@NC–ZnO	3	593	3	7200	30.6	33.1	16.9	24.3	18.6	16	[23]
Na–Fe_3O_4/HZSM-5	3	593	3	4000	22	16.6[e]	4.0	79.4	20.1	1000	[24]
$Fe_6Zn_1Al_1$–Na	3	603	1.5	15,000	39.1	24.7[g]	16.0	53.5[b]	22.5	70	[25]
0.5Na/Fe	3	593	3	2040	38.4	64[d]	7.2	NA	9.1	10	[26]
Fe–Mn–Na	3	613	2	12000[j]	35	38.7[e]	13.1	48.2	18.1	50	[28]
Fe–0.5%Na	3	563	1.5	10,000	35.3	57[f]	31.8[m]	NA	13.2	20+	[29]
K–Fe_X	3	543	0.5	2700	38	37	16	NA	12.5	75	[30]
Fe/C-bio	3	593	1	10[i]	30.5	33.2	11.8	63.9[b]	23.2	100	[36]
0.8K–2.4Fe–1.3Ti	3	593	2	1000	35.2	59.3	23.3	9.3	70.1	72	[44]
Activated $CuFeO_2$	3	593	0.1	2400	27.3	18.8[g]	5.4	66.9[h]	43.7	50	[38]
	3	573	3	1800	27.5	29.4	6.2	64.4	14.1	NA	[38]
S–3Cu10Fe1K/Al_2O_3	3	673	3	3600	38.6	2.6	28.3	9.5	36.1	5	[39]
S–10Fe3Cu1K/Al_2O_3	3	673	3	3600	40.1	2.4	26.1	10.1	36.7	5	[39]
10Fe3Cu1K/Al_2O_3	3	673	3	3600	41.7	1.6	27.8	13.8	26.5	5	[39]
10Fe3Mn1K/Al_2O_3	3	673	3	3600	42	9.4	36.1	11.1	23	5	[39]
10Fe3Mo1K/Al_2O_3	3	673	3	3600	39.2	8.2	31.1	8.9	31.3	5	[39]
10Fe3Zn1K/Al_2O_3	3	673	3	3600	38.6	7.5	35.8	6.8	33.3	5	[39]
$CuFeO_2$-6	3	573	1	1800	17.3	27.3	2.7[m]	66.3	31.7	16	[41]
$ZnFe_2O_4$	2.5	593	2	10[i]	41.3	52[e]	33.3	14.7	8.1	36	[42]
Na–$ZnFe_2O_4$	2.5	593	2	10[i]	46.7	51[e]	15.0	34.0	9.2	36	[42]
K–$ZnFe_2O_4$	2.5	593	2	10[i]	47.1	39.1[e]	14.8	46.1	8.7	36	[42]
K–$Zn(FeCo)_2O_4$	2.5	593	2	10[i]	60.4	51.3[e]	28	20.7	4.5	36	[42]

Table 1 (continued)

Catalysts	H/C	Temperature (K)	Pressure (MPa)	Space velocity (mL/(g_{cat}. h))	CO_2 conversion/%	Selectivity (%)[n]				Stability/h^c	Refs
						$C_2^= - C_4^=$	CH_4	C_{5+}	CO		
Fe_2Zn_1	3	603	1.5	15,000	43.5	18.5[a]	11.5	68.2[b]	9.2	100	[46]
FeMnKCeAl800	3	563	1.38	5400[j]	50.4	62.3[k]	22.9[m]	NA	14.8	100	[47]
K/Mn/Fe/NCNT	3	633	2.5	50,000	35	NA	25	NA	NA	60	[48]
Fe–Co/K–Al_2O_3	3	593	2	9000	49	37	23[m]	24.9	9.4	25	[51]
KZFe–5.0Co	3	593	2	6000	50.2	31.6[e]	11.3	57.8	8.1	60	[52]
FeK/Co–NC	3	573	2.5	2000	51.7	36[e]	21.6	42.4	4	100	[55]
0.8Fe–0.1K@N-OMC	3	593	3	4800	54.5	65.63	10.2	3.2	8.9	100	[59]
0.8Fe@N-OMC	3	593	3	4800	53.6	40.81	12.8	0.25	4.56	100	[59]
Fe/OCNT	3	633	2.5	50,000	26.3	2.59[l]	61.3[m]	6.21	38.8	60	[61]
Fe/NCNT	3	633	2.5	50,000	25.2	3.91[l]	62[m]	2.48	35.6	60	[61]
Fe/SiO_2	3	633	2.5	50,000	14.5	0.49[l]	75.3[m]	8.29	56.6	60	[61]
Fe/C-1EDA	3	573	1	12[i]	22.8	15.2	41.5	14.8	22.9	6	[61]
FeK/C-1EDA	3	573	1	12[i]	20.1	37.7	17.2	39.5	31.7	6	[62]
Fe–0.2Na	3	603	1.5	15,000	38.1	24.5[g]	29.4[m]	38.1[b]	15.3	30	[68]
Fe	3	603	1.5	15,000	38.9	27.1[g]	37.8[m]	24.6[b]	13.8	30	[68]

a, C_2–C_3 product selectivity; b, C_{4+} product selectivity; c, The time of the experiment; d, alkenes selectivity; e, C_2–C_4 product selectivity; f, $C_2^=$–$C_7^=$product selectivity; g, $C_2^=$–$C_3^=$product selectivity; h, $C_{4+}^=$ product selectivity; i, W/F(g h^{-1} mol^{-1}); j, h^{-1}; k, C_{2+} product selectivity; l, $C_2^=$–$C_5^=$product selectivity; m, C_1 product selectivity; n, CO excluded; o, Co-impregnation; p, Powder mixing; q, Particle mixing; r, The two catalysts were loaded into two reactors; s, Potassium modified Y molecular sieve

Zn–Fe interfaces, the CO insertion mechanism is more advantageous [38].

Conclusions and Perspectives

Using CO_2 as a feedstock for olefin production is an effective way to utilize CO_2 and reduce dependence on petroleum and natural gas. The main challenge is to achieve high selectivity toward olefins and suppress C_1 by-products (CO and CH_4). This article summarizes the recent progress on iron-based catalysts for CO_2 hydrogenation to olefins (CO_2-FTS). CO_2-FTS has made significant advancements in recent years, especially in synthesizing long-chain olefins. However, the nature of active sites, the interactions between promoters and supports, and the reaction mechanism are still debated. Improved catalysts that combine RWGS activity with chain growth are needed. Catalysts can be tailored to achieve better performance by understanding the fundamental structure–composition–activity relationship of these catalytic systems.

The performances of iron-based catalysts can be enhanced by doping transition elements such as Cu, Zn, Mn, and Co. The interaction between transition metal elements and Fe affects the formation, dispersion, and stability of active phases, especially carbides in iron-based catalysts. Enough carbide content and proper distribution can enhance C–C coupling and increase the proportion of high-carbon number products. Therefore, improving the content and distribution of carbides through interactions between Fe and second metals may be a strategy to enhance product carbon number. Alkali metals can improve the selectivity toward olefins by increasing surface electron enrichment, enhancing the surface basicity of the catalyst, and facilitating olefin desorption. Moreover, increased surface basicity favors CO_2 adsorption, leading to reduced surface H/C ratio, suppression of intermediate hydrogenation, promotion of C–C coupling, and increased olefin yield. Therefore, improving the surface basicity conditions of catalysts and increasing the number of moderately strong basic sites for CO_2 adsorption are effective ways to enhance the proportion of olefin products (Table 1).

Besides alkali metals, surface-basic nitride carbon supports can also be incorporated. The combination modes of promoter elements with Fe are also crucial for product selectivity. A well-designed structure can coordinate the carbide and oxide phases of iron better. Novel carbon materials such as carbon nanotubes and nitride carbons with new structures or special functional groups can also be explored as catalyst supports. Supports with specific spatial structures can limit the growth of active phase particle size caused by sintering and improve catalyst stability. Understanding key steps and intermediates in the reaction process through DFT calculations and stabilizing critical intermediates or lowering the energy barriers of key steps are meaningful research directions. Furthermore, it

is important to consider the influence of the support and active phase environment and design an optimal CO_2-FTS catalyst with suitable metal phases, particle sizes, and surface structures, considering the impact of support and active phase surroundings.

Acknowledgements The research is supported by the National Natural Science Foundation of China-Outstanding Youth Foundation (No. 22322814), the National Natural Science Foundation of China (No. 22108144) and the Natural Science Foundation of Shandong-Outstanding Youth Foundation (No. ZR2023YQ017)

Declarations

Conflict of interest All authors declare that there are no competing interests.

References

1. Yang S, Chun H-J, Lee S et al (2020) Comparative study of olefin production from CO and CO_2 using Na- and K-promoted zinc ferrite. ACS Catal 10(18):10742–10759
2. Guo L, Cui Y, Li H et al (2019) Selective formation of linear-alpha olefins (LAOs) by CO_2 hydrogenation over bimetallic Fe/Co-Y catalyst. Catal Commun 130:105759
3. Weifeng T, Chao S, Zhengzhou Z et al (2021) Chemical and structural properties of Na decorated Fe_5C_2–ZnO catalysts during hydrogenation of CO_2 to linear α-olefins. Appl Catal, B 298:120567
4. Do TN, Kim J (2020) Green C_2–C_4 hydrocarbon production through direct CO_2 hydrogenation with renewable hydrogen: Process development and techno-economic analysis. Energy Convers Manage 214:112866
5. Bowker M (2019) Methanol synthesis from CO_2 hydrogenation. ChemCatChem 11(17):4238–4246
6. Amrillah T, Supandi AR, Puspasari V et al (2022) MXene-based photocatalysts and electrocatalysts for CO_2 conversion to chemicals. Trans Tianjin Univ 28(4):307–322
7. Shen J, Tang R, Wu Z et al (2022) Integrated photothermal nanoreactors for efficient hydrogenation of CO_2. Trans Tianjin Univ 28(4):236–244
8. Wang Y, Zhang C, Li R (2022) Modulating the selectivity of photocatalytic CO_2 reduction in barium titanate by introducing oxygen vacancies. Trans Tianjin Univ 28(4):227–235
9. Kim Y, Song Y, Kim Y et al (2022) Multifunctional long-lived catalysts for direct hydrogenative conversion of CO_2 to liquid hydrocarbons with upscaling C_{5+} productivity. J Mater Chem A 10(41):21862–21873
10. Chen W, Lin T, Dai Y et al (2017) Recent advances in the investigation of nanoeffects of Fischer–Tropsch catalysts. Catal Today 311:8–22
11. Wang D, Xie Z, Porosoff MD et al (2021) Recent advances in carbon dioxide hydrogenation to produce olefins and aromatics. Chem 7(9):2277–2311
12. Wang X, Wu D, Zhang J et al (2019) Highly selective conversion of CO_2 to light olefins via Fischer–Tropsch synthesis over stable layered K-Fe–Ti catalysts. Appl Catal, A 573:32–40
13. Yang H, Dang Y, Cui X et al (2023) Selective synthesis of olefins via CO_2 hydrogenation over transition-metal-doped iron-based catalysts. Appl Catal, B 321:122050
14. Junhui L, Yakun S, Xuming G et al (2022) Recent advances in application of iron-based catalysts for CO_x hydrogenation to value-added hydrocarbons. Chin J Catal 43(3):731–754
15. Yongjun J, Kangzhou W, Yuan W et al (2022) Recent advances in thermocatalytic hydrogenation of carbon dioxide to light olefins and liquid fuels via modified Fischer-Tropsch pathway. J CO_2 Util 67:102321
16. Gao P, Zhang L, Li S et al (2020) Novel heterogeneous catalysts for CO_2 hydrogenation to liquid fuels. ACS Cent Sci 6(10):1657–1670
17. Yahyazadeh A, Dalai AK, Ma W et al (2021) Fischer–Tropsch synthesis for light olefins from syngas: a review of catalyst development. Reactions 2(3):227–257
18. Jiang F, Liu B, Geng S et al (2018) Hydrogenation of CO_2 into hydrocarbons: enhanced catalytic activity over Fe-based Fischer–Tropsch catalysts†. Catal Sci Technol 8(16):4097–4107
19. Yang H, Zhang C, Gao P et al (2017) A review of the catalytic hydrogenation of carbon dioxide into value-added hydrocarbons. Catal Sci Technol 7(20):4580–4598
20. Goud D, Gupta R, Maligal-Ganesh R et al (2020) Review of catalyst design and mechanistic studies for the production of olefins from anthropogenic CO_2. ACS Catal 10(23):14258–14282
21. Nasriddinov K, Min J-E, Park H-G et al (2021) Effect of Co, Cu, and Zn on FeAlK catalysts in CO_2 hydrogenation to C_{5+} hydrocarbons. Catal Sci Technol 12(3):906–915
22. Zhenyu C, Fenglei Z, Sibing Y et al (2022) PBA-derived high-efficiency iron-based catalysts for CO_2 hydrogenation. Catal Sci Technol 12(12):3826–3835
23. Liu J, Zhang A, Jiang X et al (2019) Overcoating the surface of Fe-based catalyst with ZnO and nitrogen-doped carbon toward high selectivity of light olefins in CO_2 hydrogenation. Ind Eng Chem Res 58(10):4017–4023
24. Wei J, Ge Q, Yao R et al (2017) Directly converting CO_2 into a gasoline fuel. Nat Commun 8:15174
25. Xu M, Liu X, Cao C et al (2021) Ternary Fe–Zn–Al spinel catalyst for CO_2 hydrogenation to linear α-Olefins: synergy Effects between Al and Zn. ACS Sustain Chem Eng 9(41):13818–13830
26. Liang B, Duan H, Sun T, Ma J, Liu X, Xu J, Su X, Huang Y, Zhang T (2019) Effect of Na promoter on Fe-based catalyst for CO_2 hydrogenation to alkenes. ACS Sustain Chem Eng 7(1):925–932
27. Zhai P, Xu C, Gao R et al (2016) Highly tunable selectivity for syngas-derived alkenes over zinc and sodium-modulated Fe_5C_2 catalyst. Angew Chem Int Ed 55(34):9902–9907
28. Xu Y, Zhai P, Deng Y et al (2020) Highly selective olefin production from CO_2 hydrogenation on iron catalysts: a subtle synergy between manganese and sodium additives. Angew Chem Int Ed 59(48):21736–21744
29. Wei C, Tu W, Jia L et al (2020) The evolutions of carbon and iron species modified by Na and their tuning effect on the hydrogenation of CO_2 to olefins. Appl Surf Sci 525:146622
30. Joshua Iseoluwa O, Jian W, Yu H et al (2022) Highly stable Sr and Na co-decorated Fe catalyst for high-valued olefin synthesis from CO_2 hydrogenation. Appl Catal, B 316:121640

31. Hou Y, Wang X, Chen M et al (2022) $Sr_{1-x}K_xFeO_3$ perovskite catalysts with enhanced RWGS reactivity for CO_2 hydrogenation to light olefins. Atmosphere 13(5):760
32. Joshua Iseoluwa O, Ghebretensae Aron K, Yang Y et al (2023) Emerging spinel ferrite catalysts for driving CO_2 hydrogenation to high-value chemicals. Matter 6(5):1404–1434
33. Lan Q, Jin S, Yang B et al (2022) Metal-oxo cluster catalysts for photocatalytic water splitting and carbon dioxide reduction. Trans Tianjin Univ 28(3):214–225
34. Visconti CG, Martinelli M, Falbo L et al (2016) CO_2 hydrogenation to lower olefins on a high surface area K-promoted bulk Fe-catalyst. Appl Catal, B 200:530–542
35. Shafer WD, Jacobs G, Graham UM et al (2018) Increased CO_2 hydrogenation to liquid products using promoted iron catalysts. J Catal 369:239–248
36. Guo L, Sun J, Ji X et al (2018) Directly converting carbon dioxide to linear α-olefins on bio-promoted catalysts. Commun Chem 1:11
37. Tian P, Gu M, Qiu R et al (2021) Tunable carbon dioxide activation pathway over iron oxide catalysts: effects of potassium. Ind Eng Chem Res 60(24):8705–8713
38. Li Z, Wu W, Wang M et al (2022) Ambient-pressure hydrogenation of CO_2 into long-chain olefins. Nat Commun 13:2396
39. Liu J, Zhang A, Jiang X et al (2018) Selective CO_2 hydrogenation to hydrocarbons on Cu-promoted Fe-based catalysts: dependence on Cu–Fe interaction. ACS Sustain Chem Eng 6(8):10182–10190
40. Jiang G, Han D, Han Z et al (2022) Rational manipulation of intermediates on copper for CO_2 electroreduction toward multicarbon products. Trans Tianjin Univ 28(4):265–291
41. Choi YH, Jang YJ, Park H et al (2017) Carbon dioxide Fischer–Tropsch synthesis: A new path to carbon-neutral fuels. Appl Catal, B 202:605–610
42. Guo L, Li J, Cui Y et al (2020) Spinel-structure catalyst catalyzing CO_2 hydrogenation to full spectrum alkenes with an ultra-high yield. Chem Commun 56(65):9372–9375
43. Wu D-K, Wang X, Gao X-H et al (2019) Preparation of layered K–Fe–Zn–Ti catalyst and its performance in the hydrogenation of carbon dioxide to light olefins. J Fuel Chem Technol 47(8):949–956
44. Yang S, Lee S, Kang SC et al (2019) Linear α-olefin production with Na-promoted Fe–Zn catalysts via Fischer–Tropsch synthesis. RSC Adv 9(25):14176–14187
45. Liu S, Zhao Q, Han X et al (2023) Proximity effect of Fe–Zn bimetallic catalysts on CO_2 hydrogenation performance. Trans Tianjin Univ 29(4):293–303
46. Zhang C, Xu M, Yang Z et al (2021) Uncovering the electronic effects of zinc on the structure of Fe_5C_2-ZnO catalysts for CO_2 hydrogenation to linear α-olefins. Appl Catal, B 295:120287
47. Dorner RW, Hardy DR, Williams FW et al (2011) C_2–C_{5+} olefin production from CO_2 hydrogenation using ceria modified Fe/Mn/K catalysts. Catal Commun 15(1):88–92
48. Kangvansura P, Chew LM, Saengsui W et al (2016) Product distribution of CO_2 hydrogenation by K- and Mn-promoted Fe catalysts supported on N-functionalized carbon nanotubes. Catal Today 275:59–65
49. Liang B, Sun T, Ma J et al (2018) Mn decorated Na/Fe catalysts for CO_2 hydrogenation to light olefins†. Catal Sci Technol 9(2):456–464
50. Li M, Shen L, Yang M-Q (2022) Cobalt-based cocatalysts for photocatalytic CO_2 reduction. Trans Tianjin Univ 28(6):506–532
51. Numpilai T, Witoon T, Chanlek N et al (2017) Structure–activity relationships of Fe–Co/K–Al_2O_3 catalysts calcined at different temperatures for CO_2 hydrogenation to light olefins. Appl Catal, A 547:219–229
52. Lisheng G, Xinhua G, Weizhe G et al (2022) High-yield production of liquid fuels in CO_2 hydrogenation on a zeolite-free Fe-based catalyst. Chem Sci 4(1):171–178
53. Li S, Ren P, Yang C et al (2018) Fe_5C_2 nanoparticles as low-cost HER electrocatalyst: the importance of Co substitution. Sci Bull 63(20):1358–1363
54. Calizzi M, Mutschler R, Patelli N et al (2020) CO_2 hydrogenation over unsupported Fe–Co nanoalloy catalysts. Nanomaterials 10(7):1360
55. Hwang S-M, Han SJ, Park H-G et al (2021) Atomically alloyed Fe–Co catalyst derived from a N-Coordinated Co single-atom structure for CO_2 hydrogenation. ACS Catal 11(4):2267–2278
56. Kim KY, Lee H, Noh WY et al (2020) Cobalt ferrite nanoparticles to form a catalytic Co–Fe alloy carbide phase for Selective CO_2 hydrogenation to light olefins. ACS Catal 10(15):8660–8671
57. Visconti CG, Martinelli M, Falbo L et al (2016) CO_2 hydrogenation to hydrocarbons over Co and Fe-based Fischer-Tropsch catalysts. Catal Today 277:161–170
58. Sonal N, Kondamudi K, Pant KK et al (2017) Synergistic effect of Fe–Co bimetallic catalyst on FTS and WGS activity in the Fische–Tropsch process: a kinetic study. Ind Eng Chem Res 56(16):4659–4671
59. Pengze Z, Fei H, Jingyu Y et al (2021) N-doped ordered mesoporous carbon (N-OMC) confined Fe_3O_4-FeC_x heterojunction for efficient conversion of CO_2 to light olefins. Appl Catal, B 299:120639
60. Ji Y, Du J, Chen A (2022) Review on heteroatom doping carbonaceous materials toward electrocatalytic carbon dioxide reduction. Trans Tianjin Univ 28(4):292–306
61. Chew LM, Kangvansura P, Ruland H et al (2014) Effect of nitrogen doping on the reducibility, activity and selectivity of carbon nanotube-supported iron catalysts applied in CO_2 hydrogenation. Appl Catal, A 482:163–170
62. Kosol R, Guo L, Kodama N et al (2020) Iron catalysts supported on nitrogen functionalized carbon for improved CO_2 hydrogenation performance. Catal Commun 149:106216
63. Chen W, Fan Z, Pan X et al (2008) Effect of confinement in carbon nanotubes on the activity of Fischer−Tropsch iron catalyst. J Am Chem Soc 130(29):9414–9419
64. Guo L, Zhang P, Cui Y et al (2019) One-pot hydrothermal synthesis of nitrogen functionalized carbonaceous material catalysts with embedded iron nanoparticles for CO_2 hydrogenation. ACS Sustainable Chem Eng 7(9):8331–8339
65. Torres Galvis HM, Koeken ACJ, Bitter JH et al (2013) Effects of sodium and sulfur on catalytic performance of supported iron catalysts for the Fischer–Tropsch synthesis of lower olefins. J Catal 303:22–30
66. Wu B, Bai L, Xiang H et al (2004) An active iron catalyst containing sulfur for Fischer–Tropsch synthesis. Fuel 83(2):205–212
67. Torres Galvis HM, Bitter JH, Khare CB et al (2012) Supported iron nanoparticles as catalysts for sustainable production of lower olefins. Science 335(6070):835–838
68. Xu M, Cao C, Xu J (2022) Understanding kinetically interplaying reverse water-gas shift and Fischer–Tropsch synthesis during CO_2 hydrogenation over Fe-based catalysts. Appl Catal, A 641:118682
69. Han SJ, Hwang S-M, Park H-G et al (2020) Identification of active sites for CO_2 hydrogenation in Fe catalysts by first-principles microkinetic modelling. J Mater Chem A 8(26):13014–13023
70. Huang J, Jiang S, Wang M et al (2021) Dynamic evolution of Fe and carbon species over different ZrO_2 supports during CO prereduction and their effects on CO_2 hydrogenation to light olefins. ACS Sustain Chem Eng 9(23):7891–7903
71. Nie X, Han G, Song C et al (2022) Computational identification of facet-dependent CO_2 initial activation and hydrogenation over iron carbide catalyst. J CO_2 Util 59:101967
72. Visconti CG, Lietti L, Tronconi E et al (2008) Fischer–Tropsch synthesis on a Co/Al_2O_3 catalyst with CO_2 containing syngas. Appl Catal, A 355(1–2):61–68

73. Wang H, Nie X, Liu Y et al (2022) Mechanistic insight into hydrocarbon synthesis via CO_2 hydrogenation on χ-Fe_5C_2 catalysts. ACS Appl Mater Interfaces 14(33):37637–37651
74. Nahuel Moreno Y, Pablo LDQ, Víctor AR (2023) A DFT study on the adsorption and dissociation of N-Nitrosodimethylamine on a Ni_8 nanocluster. J Mol Graphics Modell 125:108578
75. Gunasooriya GTKK, van Bavel AP, Kuipers HPCE et al (2016) Key role of surface hydroxyl groups in C–O activation during Fischer–Tropsch synthesis. ACS Catal 6(6):3660–3664
76. Saeidi S, Najari S, Fazlollahi F et al (2017) Mechanisms and kinetics of CO_2 hydrogenation to value-added products: a detailed review on current status and future trends. Renew Sustain Energy Rev 80:1292–1311
77. Fischer F, Tropsch HJB-C (1926) The synthesis of petroleum at atmospheric pressures from gasification products of coal. Brennstoff-Chem 7:97–104
78. van Santen RA, Ghouri MM, Shetty S et al (2011) Structure sensitivity of the Fischer–Tropsch reaction; molecular kinetics simulations. Catal Sci Technol 1(6):891–911
79. Thanh Hai P, Xuezhi D, Gang Q et al (2014) CO activation pathways of Fischer–Tropsch synthesis on χ-Fe_5C_2 (510): direct versus hydrogen-assisted CO dissociation. J Phys Chem C 118(19):10170–10176
80. Huo C-F, Li Y-W, Wang J et al (2009) Insight into CH_4 formation in Iron-catalyzed Fischer−Tropsch synthesis. J Am Chem Soc 131(41):14713–14721
81. Ojeda M, Nabar R, Nilekar AU et al (2010) CO activation pathways and the mechanism of Fischer–Tropsch synthesis. J Catal 272(2):287–297
82. Cheng J, Hu P, Ellis P et al (2008) A first-principles study of oxygenates on co surfaces in Fischer−Tropsch synthesis. J Phys Chem C 112(25):9464–9473
83. Cao D-B, Li Y-W, Wang J et al (2011) Chain growth mechanism of Fischer–Tropsch synthesis on Fe_5C_2(0 0 1). J Mol Catal A: Chem 346(1–2):55–69
84. Gracia JM, Prinsloo FF, Niemantsverdriet JW (2009) Mars-van Krevelen-like mechanism of CO hydrogenation on an iron carbide surface. Catal Lett 133(3):257–261
85. Davis BH (2008) Fischer–Tropsch synthesis: reaction mechanisms for iron catalysts. Catal Today 141(1–2):25–33
86. Gaube J, Klein HF (2009) Further support for the two-mechanisms hypothesis of Fischer–Tropsch synthesis. Appl Catal, A 374(1–2):120–125
87. Yin J, Liu X, Liu X-W et al (2020) Theoretical exploration of intrinsic facet-dependent CH_4 and C_2 formation on Fe_5C_2 particle. Appl Catal, B 278:119308

Yuling Shan received his Ph.D. degree from East China University of Science and Technology in 2016. Currently, he is an associate professor at Qingdao University of science and technology since 2018. His research focuses on the design and synthesis of supported metal and metal oxide catalysts, and their applications in CO2 hydrogenation and alkane dehydrogenation.

Xiang Feng received his B.Sc. and Ph.D. degrees from East China University of Science and Technology in 2010 and 2015, respectively. Then he worked as Postdoctoral Research Fellow at Norwegian University of Science and Technology. He is currently a Professor at the China University of Petroleum. His research interests are mainly focused on manipulating the micro-nano scale structures of industrial catalysts to develop highly efficient and stable catalysts and their application in green synthesis of high-value Chemicals.